Excerpts from Ph231 Particle Physics Phenomenology Notes

This course was taught ~1983 at Caltech by Geoffrey Fox.

The full notes and lots of problem sets are available

Part VIII Times Gone By: The S Matrix Era

See section IVF later in excerpt for Kinematics and Mandelstam variables
See section VI.H E350 and VI.I E110 and E350 in excerpt for discussion of experiments
Note even in early 1980's, I viewed S matrix theory as past!

A: Introduction

- Why in 1960-1970 did we do S Matrix theory and not QFT

B: Analyticity and Mandelstam variables s t u

- See part IVF of notes
- Analyticity structure for spinless π p scattering

C: Generalized Unitarity

- Discontinuities and cuts of various types
- Watson's theorem

D: Analyticity in Quantum Field Theory; Dispersion Relations

- Crossing
- Dispersion Relation**s**
- t=0 dispersion relations for elastic scattering involves total cross section
- Measure real part by coulomb interference
- Subtractions
- Froissart bound
- Resonances in dispersion relations
- π^+ p fixed t dispersion relations
- pn $\rightarrow$ pn fixed s dispersion relations and pion pole

E: Determination of Singularities of Analytic Functions represented in integral form

- Chapter 2 of ELOP
- Analysis of pinches causing singularities
- Two cases considered
- Quark Propagator
- Box diagram

F: The Mandelstam Representation and his Iteration

- Potential theory; representation of amplitude as double integral over double spectral function plus poles
- Relativistic generalization with 3 spectral functions and poles

- Why you can (in principle) calculate amplitude from unitarity and analyticity in potential theory and why it breaks down due to multichannel effects in relativistic problem

G. Regge Theory

- Derivation of basic pole expansion at large z
- Remarks on potential theory where poles go to -1 and large z limit irrelevant
- Why more important in QFT as captures effect of crossed reactions
- Simple examples referencing Fox&Quigg and dominant q-qbar Regge poles
- Signature and why it is important in QFT and not in potential theory
- Ladder diagrams and Regge Poles
- Glueballs and Pomeron
- Relation of Regge and high p-transverse limits
- Analysis of Feynman graphs and how they generate poles from ladder graphs
- Box diagrams and the absorption model generating cuts. Analysis of reliability of this
- Triple Regge Theory
- See experiment E350 described in Section VI-H,

H Duality, Finite Energy Sum Rules, the Veneziano Model

- Derivation of FESR from Dispersion relations and Regge theory
- $\pi^+ \pi^0 \rightarrow \pi^+ \pi^0$ to illustrate bootstrap
- Duality. Resonances include Regge
- Veneziano model
- Exchange degeneracy
- 2-component duality

I Low Transverse Momentum Physics (see Picture Book)

- See experiment E110 and E260 described in Section VI-I
- Quasi 2 body
- Diffraction -- elastic excitation (beam, target, both), Deck effect, Pomeron Triple Regge
- Multi particle: pion multiplicity, low pT, multiperipheral, quark cascades, independent pion spray, relation to QCD, Mueller

VIII. The S-Matrix Era: Analyticity, Unitarity, Duality, Regge Theory, the Bootstrap.

VIII.A. Introduction

We now discuss a set of topics that were the forefront of theoretical high energy physics 10 years ago. They share property of being true in nearly all quantum field theories (sometimes only proved true in perturbation theory). In those far off days it did not seem likely that one could ever solve a quantum field theory (or even get physics out of it). Thus the popular approach was to abstract from QFT general properties and study these instead. These ideas culminated in the bootstrap principle which supposed that all of hadron dynamics could be deduced from these general properties plus some assumptions which corresponded physically to the lack of elementary particles. (At that time quarks were not popular and all the known hadrons showed, as now, every evidence of being composite.)

The discovery of asymptotic freedom has shown that it is in fact possible to calculate (successfully we claim) the predictions of a QFT, i.e. QCD; further this success strongly suggests that there are elementary particles (quarks and gluons). Thus both the original motivation and one of basic assumptions of the bootstrap have been cast into doubt. To make matters worse, we were never able to do significant calculations in the bootstrap approach. However it is still true that the general techniques developed in these years are very useful - simply because they are correct properties of QCD. Some references are:

P. Collins, "An Introduction to Regge Theory and High Energy Physics."

R. J. Eden, "High Energy Collisions of Elementary Particles."

R. J. Eden, P. V. Landshoff, D. I. Olive, J. C. Polkinghorne, "The Analytic S-Matrix," (ELOP).

I shall also use an old set of notes of mine - called "Picture Book of High Energy Scattering," of PB for short.

VIII.B. Analyticity

We have already introduced this in IV.F and again we shall take two body → two body scattering. The scattering amplitude A(s,t,u) is an analytic function of s, t and u; $s + t + u = \sum_i m_i^2$. The same function of these invariants describes 3 distinct processes

$a + b \to c + d$	s channel
$a + \bar{c} \to \bar{b} + d$	u channel
$a + \bar{d} \to c + \bar{b}$	t channel

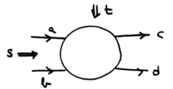

The variable in the this column is c.m. energy^2 for the three processes. This is illustrated on p. 9 of PB for the case $a = \pi^+$ $b = p$ and $c = \pi^+$ $d = p$. Note the physical regions for the three processes are distinct areas in s, t, u space and this relation between the three leads to <u>no direct</u> physical relations between scattering amplitudes because one must use analytic continuation to relate the amplitudes. The simplest way of doing this is through dispersion relations. These are not described in Perkins but they are done in Mathews and Walker (chapter 5). We will go through this for illustrated case of πp scattering but I will ignore <u>spin</u> of particles, i.e. protons. This does not in fact affect the argument in any essential way.

We need to discuss the singularities of A(s,t) where we drop argument u as

$$u = 2m^2 + 2\mu^2 - s - t$$

m is proton mass, μ is π mass.

The analytic function (note analytic does not imply regular everywhere) $A(s,t)$ has singularities from two basic mechanisms.

(1) $A(s,t)$ has poles corresponding to stable (we switch off electromagnetic and weak interactions for convenience) single particle diagrams. In $\pi^+p \to \pi^+p$ there is only one such case. Namely

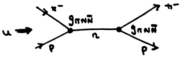

Notice this is a u channel diagram. The contribution of this diagram to $A(s,t)$ is

$$\frac{c}{m_n^2 - u}$$

As you know from Feynman rules c can be related to square of π nucleon coupling constant $g^2/4\pi \sim 14.5$ (This is g for $\pi^0 p\bar{p}$ coupling.) Notice this is much larger than $q\bar{q}g$ coupling at $Q^2 = 1\ \text{GeV}^2$ (where $g^2/4\pi \sim 1$). Probably it should be compared with $q\bar{q}g$ coupling at $Q^2 = (300\ \text{MeV})^2$ but unfortunately there is no way of estimating this.

(2) $A(s,t)$ has cuts starting at all thresholds for physical particle processes. For instance $\pi^+p \to \pi^+p$ has a cut at

$s = (m + \mu)^2$, corresponding to

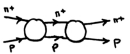

$s = (m + 2\mu)^2$, corresponding to

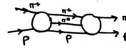

$s = (m_K + m_\Sigma)^2$, corresponding to

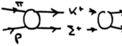

We draw all (clearly there are an infinity of them!) cuts from starting position to $+\infty$. Then they overlap and we need only worry about cut with lowest threshold

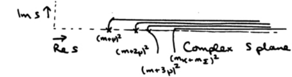

Note that the pole (i) can be regarded as a special case (with but one intermediate particle) of the cut (ii). Namely general statement on singularity structure of A is that: Singularities correspond to the existence of intermediate states containing real particles. If it is a one particle intermediate state, then one has a pole but if two or more particles, one gets a cut.

As we will see later unitarity can be used to relate size of singularity ("size" is residue for pole, discontinuity for cut) in ab → cd to product of amplitudes for ab → n and n → dc. This gives cut corresponding to intermediate state "n" - one must sum over all intermediate states n to get total discontuniuty over cut. For a pole we already see this with residue being proportional to product of coupling constants specifying amplitudes

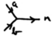

and

The above remarks are the basis of the "physical" basis of the analyticity of amplitudes. Namely all singularities are consequences of intermediate states iterated by unitarity. Actually this is not always true but it is believed to be valid in cases of interest.

Unitarity relates the imaginary part of the amplitude A (for initial state i goes to final state f) to a sum over intermediate states n, i.e.

$$S^{+}S = 1 \qquad \text{(s matrix)}$$

$$S = 1 + iA \qquad \text{(A is T matrix)}$$

$$\therefore \quad 2\,\mathrm{Im}\,A(i \to f) = \sum_{n} A(i \to n)\,A^{*}(f \to n) \qquad (1)$$

where we used time reversal invariance which says A is a symmetric matrix. Now in (1), we see that Im A changes at each threshold because a new state n is added to the sum on left hand side. Thus it is obvious that singularities (cuts) are associated with thresholds. The above argument does not of course show that the threshold induced singularities are the only singularities on the physical sheet.

We should also dicusss resonances at this point. We have learned that these can be considered as particles with mass $m - i\Gamma_R/2$ and so the s channel diagram

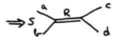

has the form:

$$\frac{c}{s - m^2 + i\Gamma_R m} \quad , \qquad \text{neglecting } \Gamma_R^2 . \tag{2}$$

This is a pole at $s = m^2 - i\Gamma_R m$ (3)

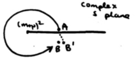

Now because a resonance decays it is always above some threshold and so in cut region. We can reach (2) in two ways. One by starting just above cut (at A above) and preceding down to B'. Alternately we can round singularity and arrive at B. B and B' have same s value but amplitude differs. In fact A is singluar at B' (i.e. has resonance pole) but <u>not</u> B. B' is on "second sheet" gotten by going through cut. B is on "physical sheet." This is a general result; the only physical sheet singularities are (i) poles below threshold and (ii) cuts. There are no other stray poles or cuts.

The lack of singularity of (i) at B follows (in simplest case) because

Γ_R should (approximately) be replaced by $\Gamma_R p(s)/p(s_R)$ where p is c.m. momenta $\alpha\sqrt{s - (m + \ )^2}$. Comparing B and B', p(s) reverses sign and so nature avoids a singularity at B. Note that p(s) in (2) now does give it a cut at $s = (m + \mu)^2$. Further for s real and $< (m + \mu)^2$, p(s) is purely imaginary and the form (2) becomes purely real. This is a general result called "Hermitean analyticity" (only true if time reversal is a valid symmetry and for same phase conventions that give (1)) - namely

$$A(s^*) = A^*(s) \tag{4}$$

where * is complex conjugation.

Taking as above s real and not in region of cut, A is single valued and so (4) implies that A is real there. On the cut we consider $s_A = \mathrm{Re}s + i\varepsilon$ and $s_B = \mathrm{Re}s - i\varepsilon$, where ε is an arbitrary small positive real number (A = above, B = below cut)

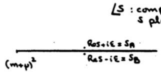

Because A is multivalued on cut, $A(s_A)$ and $A(s_B)$ are distinct and (4) simply says

$$A(s_A) = A^*(s_B)$$

i.e.
$$\mathrm{Re}A(s_A) = \mathrm{Re}A(s_B)$$
$$\mathrm{Im}A(s_A) = -\mathrm{Im}A(s_B) \tag{5}$$

We can illustrate thus for some simple mathematical functions obeying (4)

(1) $$A = \alpha - \beta\sqrt{(m+\mu)^2 - s} \qquad \alpha,\beta \text{ real}$$

$$A(s_A) = \alpha + i\beta\sqrt{s-(m+\mu)^2}$$

$$A(s_B) = \alpha - i\beta\sqrt{s-(m+\mu)^2}$$

This example is important because the cut corresponding to a 2 particle threshold is indeed of square root type. This means that A is double valued or that if you go through the cut twice you end up at the same place.

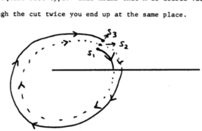

i.e. $A(s_1) = A(s_2^*) = A(s_3)$

In the above picture the solid line is the physical sheet; the dotted line is the unphysical sheet.

(2) $$A = \alpha - \beta \log[(m+\mu)^2 - s] \qquad \alpha,\beta \text{ real}$$

$$A(s_A) = \alpha - \beta \log[s-(m+\mu)^2] + i\pi\beta + 2\pi n\beta$$

$$A(s_B) = \alpha - \beta \log[s-(m+\mu)^2] - i\pi\beta - 2\pi ni\beta.$$

Here n is an integer telling you how many times you have circled cut. $n = 0$ is physical sheet and in above figure s_i has $n = i - 1 (i = 1,2,3)$. For the logarithmic singularity one never gets back to the physical sheet by circling $s = (m + \mu^2)$ as n just de-increments by 1 each time. This function has an infinite number of unphysical sheets. In nature, a three particle threshold (which after decomposition of two of the particles into total J states clearly corresponds to an infinite number of two particle thresholds) has an infinite number of unphysical sheets.

VIII.C. Generalized Unitarity

For any reaction the physical amplitude $A(s,t)$ is gotten by evaluating the associated analytic function at $s + i\varepsilon$ (s real, ε positive of course!) above all threshold cuts. This follows from the $i\varepsilon$ prescription used to interpret (regularize) the Feynman diagram propagators $1/(p^2 - m^2 + i\varepsilon)$.

Combining (1) and (4) we see that the discontinuity of $A(i \to f)$ across the cut, $s \geq (m + \mu)^2$ is just

$$2i \sum_n A(i \to n)A^*(f \to n) \tag{6}$$

Actually we can now state unitarity in a little more precise fashion; namely the discontinuity across the cut in $A(i \to f)$ corresponding to a particular intermediate state n (e.g. $K^+\Sigma^+$ or $\pi^+\pi^0 p$) is just (6) without the sum over n. Naive unitarity just gives us the total discontinuity over all cuts.

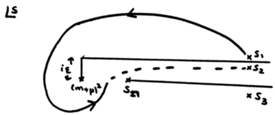

This is illustrated above for the case of two thresholds. [$s = (m + \mu)^2$ and $s = s_n$]. I have separated the threshold cuts by a small amount $i\varepsilon$ in complex s plane - normally they are drawn on top of each other. Then

$A(s_1) - A(s_3)$ is given by normal unitarity

$A(s_1) - A(s_2)$ is given by elastic term in unitarity relation

$A(s_2) - A(s_3)$ is given by term in unitarity relation corresponding to intermediate state n.

This so called generalized unitarity relation also applies to multiparticle amplitudes. Consider the reaction

$$a + b \rightarrow 1 + 2 + 3$$

and let p_i ($i = a,b,1,2,3$) be the particle momenta ($p_i^2 = m_i^2$). This amplitude is again an analytic function of the various invariants which include s_{ab}, s_{12}, s_{13} and s_{23} [$s_{12} + s_{13} + s_{23} = s_{ab} + m_1^2 + m_2^2 + m_3^2$ and $s_{ij} = (p_i + p_j)^2$]. The physical amplitude is as usual gotten by evaluating s_{ij} with $+i\varepsilon$ imaginary part. The function has threshold cuts at

$$s_{ab} = (m_a + m_b)^2 \quad \text{or} \quad (m_1 + m_2 + m_3)^2$$

$$s_{12} = (m_1 + m_2)^2 \quad \text{etc.}$$

According to generalized unitarity the discontinuity across the s_{12} cut is proportional to

$$A(ab \rightarrow 1 + 2 + 3) \times A^*(12 \rightarrow 12) \tag{1}$$

which is represented schematically below.

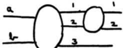

We can use this to derive "Watson's theorem" - a result that is normally gotten from "final state interaction" theory. We will first derive the theorem for the simpler case of $\gamma N \to \pi N$. This amplitude has γN and πN thresholds; however, the former can be neglected as long as we work to lowest order in e. The discontinuity across the πN cut is given by VIII.B.(1)

$$\text{Im } A(\gamma N \to \pi N) = A(\gamma N \to \pi N)\, A^*(\pi N \to \pi N) \qquad (2)$$

with a normalization such that $A(\pi N \to \pi N) = e^{i\delta} \sin\delta$. The solution of (2) is that $A(\gamma N \to \pi N)$ has same phase ($e^{i\delta}$) as the strong interaction amplitude $A(\pi N \to \pi N)$. This is the content of Watson's theorem which (after modification for violation of time reversal invariance) applies to $K \to 2\pi$ and other hadronic weak decays. [In $K \to 2\pi$, Watson's theorem says this weak interaction amplitude has the same phase as $\pi\pi \to \pi\pi$ at an s value $= m_K^2$]. A strong interaction amplitude like $A(\pi N \to \pi N)$ satisfies a non-linear unitarity relation

$$\text{Im } A(\pi N \to \pi N) = |A(\pi N \to \pi N)|^2 \qquad (3)$$

(exact below $\pi\pi N$ threshold).

with solution

$$A(\pi N \to \pi N) = e^{i\delta} \sin \delta \qquad (4)$$

for arbitary δ. Watson's theorem is the solution of the <u>linear</u> unitarity relation (2). This linear relation occurs in any "small" amplitude whose square can be neglected. However we see that the purely strong interaction process $ab \rightarrow 1 + 2 + 3$ satisfies the linear relation (2) for the "part" of unitarity corresponding to discontinuity across $s_{12} = (m_1 + m_2)^2$ cut. We deduce that $ab \rightarrow 1 + 2 + 3$ has "phase" $e^{i\delta_{12}}$ (δ_{12} phase of $1 + 2 \rightarrow 1 + 2$) from s_{12} threshold. This is a not very useful result unless we know that other sources of phases (s_{ab}, s_{13} or s_{23} cuts) are either negligible or perhaps vary slowly with s_{12} so that $e^{i\delta_{12}}$ does correctly give the s_{12} variation of the phase of $a + b \rightarrow 1 + 2 + 3$. We see that the generalized unitarity relation has enabled us to interpret final state interaction theory in a case where there are several particles interacting with each other.

VIII.D. Analyticity in Quantum Field Theory; Dispersion Relations

The discussion so far has been applicable to both non-relativistic (potential scattering) and relativistic (field theory) scattering. However we have omitted an important feature of the relativistic case coming from the existence of 3 channels described by the same amplitude. (In the non-relativistic case, only one channel is described by our amplitude.) Namely unitarity does still give all the singularities but one must add those coming from unitarity in any of the 3 channels.

Let us take as an example $A(s,t)$ for $\pi^+p \to \pi^+p$ evaluated at $t=0$ and considered as a function of the complex variable s.

$$\text{Put } f(s) = A(s,t=0) \tag{1}$$

in the non-relativistic case, $f(s)$ would just have a cut for $s \geq (m+\mu)^2$

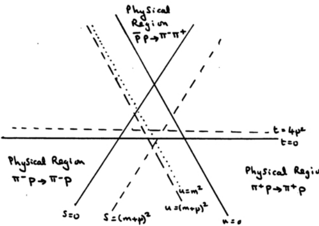

but in the field theory case we also have poles and cuts from the u and t channels. As t is fixed = 0 , we can only get the u channel contribution. This gives a cut for

$$u \geq (m + \mu)^2 \text{ or } s \leq (m - \mu)^2$$

and a pole (the neutron) at

$$u = m^2 \text{ or } s = m^2 + 2\mu^2.$$

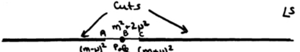

Hermitean analyticity still implies that f(s) is real in the cut free region AC and that the discontinuity of f across either cut is 2i x its imaginary part. For $s \geq (m + \mu)^2$ this discontinuity can be calculated from $\pi^+p \to \pi^+p$ unitarity and for $s \leq (m - \mu)^2$ from $\pi^-p \to \pi^-p$ unitarity. Note that the physical amplitude is $s + i\varepsilon$ (above cut) for $\pi^+p \to \pi^+p$, $s \geq (m + \mu)^2$ and $s = 2m^2 + 2\mu^2 - u - i\varepsilon$ (below cut), for $\pi^-p \to \pi^-p$, $u \geq (m + \mu)^2$. We call the two cuts the left ($s \leq (m - \mu)^2$) and right ($s \geq (m + \mu)^2$) hand cuts. The presence of the left hand cut is characteristic of field theory.

Now we can derive dispersion relations as an elementary application of Cauchy's theorem.

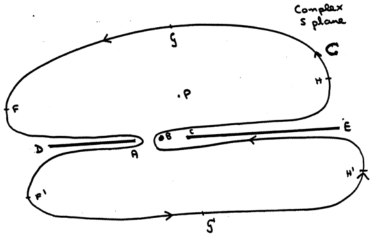

Consider

$$I = \int_C \frac{ds' f(s')}{(s' - s)} \qquad (2)$$

where s is some fixed point P. C is a contour including P but such that all singularities of f be outside it. C is transversed anti-clockwise. Then we can use Cauchy's theorem to evaluate I = $2\pi i$ x sum of residues at poles,

i.e., $\quad I = 2\pi i\, f(s) \qquad (3)$

However we can also evaluate f in a different way - namely we press bits of C like DA, CE along real axis and make the arcs FGH, FG'H' semi-circles at ∞.

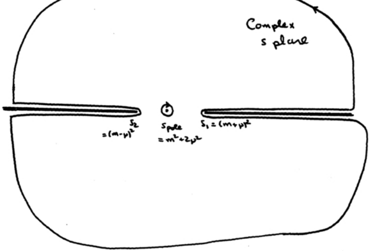

We have also split off part of integral as a little circle around the pole $s = s_{pole}$. Now

(i) The semi circle will give zero as long as $f(s')$ in (2) tends to zero fast enough at ∞. We need

$$|f(s')| \times \frac{2\pi |s'|}{|s'|} \to \text{perimeter of semi-circle} \to 0$$

$$\text{i.e. } |f| \to 0 \tag{4}$$

(ii) The pole contribution gives

$$\int_{\text{clockwise contour about } s'=s_{pole}} \frac{ds'}{(s'-s)} \frac{C'}{(s_{pole}-s')}$$

$$= 2\pi i\, C'/(s_{pole}-s) \qquad \begin{array}{l} C' = -C \text{ if} \\ f = c/m^2 - u \end{array} \tag{5}$$

(iii) The cut contribution gives

$$\int_{s_1}^{\infty} \frac{ds'}{(s'-s)} \underbrace{\{f(s'+i\varepsilon) - f(s'-i\varepsilon)\}}$$

$$+ \int_{-\infty}^{s_2} \frac{ds'}{(s'-s)} \underbrace{\{f(s'+i\varepsilon) - f(s'-i\varepsilon)\}} \tag{6}$$

But this is discontinuity across cut which is just $2i \operatorname{Im} f(s')$.

$\therefore$ equating (3) to (5) plus (6) gives

$$2\pi i\, f(s) = \frac{2\pi i\, C'}{s_{pole}-s} + 2i \left\{ \int_{s_1}^{\infty} \frac{ds'}{s'-s} \operatorname{Im} f(s') + \int_{s_2}^{\infty} \frac{du'}{u'-u} \operatorname{Im} f(u') \right\}$$

i.e.

$$f(s) = \frac{C'}{s_{pole}-s} + \frac{1}{\pi} \int_{s_1}^{\infty} \frac{ds'}{s'-s} \operatorname{Im} f(s') + \frac{1}{\pi} \int_{u_1}^{\infty} \frac{du'}{u'-u} \operatorname{Im} f(u') \tag{7}$$

Here $u' = 2m^2 + 2\mu^2 - s'$, $u_1 = 2m^2 + 2\mu^2 - s_2$, $u' - u = -(s'-s)$, $du' = -ds'$

$\operatorname{Im} f(u') = -\operatorname{Im} f(s')$: this is just conventional as $f(u'+i\varepsilon) = f(s'-i\varepsilon)$, etc.

So f is expressed as:

(i) Sum over poles whose residues are just (Feynman Diagram) coupling constants.

(ii) Integral over left and right-hand cuts. The right-hand cut corresponds to s channel discontinuity; the left-hand cut to u channel.

The dispersion relation can be derived for arbitrary t values. However there is a special simplification for t=0. Thus the unitarity relation* reads for elastic scattering $1 + 2 \to 1 + 2$

$$2 \, \mathrm{Im}\langle 12| \, A \, |12\rangle = \sum_n |\langle 12| \, A \, |n\rangle|^2 \qquad (8)$$

Now t=0 is precisely the case when initial and final state are identical.

∴ The above relation reads:

Imaginary part of forward scattering amplitude is proportional to total cross section (which is clearly $\sum_n |\langle 12|T|n\rangle|^2$). This is famous optical theorem. I say "proportional to" because (8) leaves out sundry phase space factors and in my normal conventions

$$\mathrm{Im}\, A(12 \to 12{:}\ s,\ t=0) = 2\sqrt{s}\, p_{cms}\sigma_{tot}(1 + 2 \to \text{anything}) \quad (9)$$

where p_{cms} is cms momentum in $1 + 2 \to 1 + 2$.

As both s and u channel are elastic scattering, I can replace Im A(s,t=0) = Im f(s) in (7) by the total cross section. Thus (given I can find residue at pole) have in (7) a formula for f(s) for arbitrary s in terms of experimentally measured cross sections - in our case σ_{tot} $(\pi^+ p)$ for right-hand cut and σ_{tot} $(\pi^- p)$ on left-hand cut. This relation can be checked experimentally by taking s to be on the cut. Then f(s) is the measured amplitude for say, $\pi^+ p \to \pi^+ p$. The "imaginary part of the dispersion relation" says nothing but

---

*Note that (8) is unitarity for A(s,t), i.e. states $|12\rangle, |n\rangle$ in (8) are eigenstates of the individual momenta for $|1\rangle$ and $|2\rangle$. In VIII.C (1) → (4), we are using total angular momentum eigenstates which diagonalize the unitarity relation.

but real part is non-trivial

$$\mathrm{Re}\ f(s) = \underbrace{\frac{C'}{s_{\mathrm{pole}} - s} + \frac{1}{\pi} \int_{u_1}^{\infty} \frac{du'\ \mathrm{Im}\ f(u')}{u' - u}}_{\text{these two terms are clearly real}}$$

$$+ \underbrace{\frac{1}{\pi}\, P \int_{s_1}^{\infty} \frac{ds'}{s' - s}\ \mathrm{Im}\ f(s')}$$

$$= \lim_{\varepsilon \to 0} \int_{s_1}^{s-\varepsilon} \int_{s+\varepsilon}^{\infty} \frac{ds'}{s' - s}\ \mathrm{Im}\ f(s') \qquad (10)$$

P stands for principal value - it is described in Mathews and Walker.

Thus we can predict real part in terms of total sections. The real part can be measured experimental in two ways:

(1) Measure Im $f(s) = A(s,t=0)$ from total π^+p cross section.

Measure $|\mathrm{Re} f|^2 + |\mathrm{Im}\ f|^2$ by extrapolating to $t=0$ the measured π^+p elastic differential cross section $d\sigma/dt$. By subtraction we find modulus but not sign of Ref. However the real problem with this method is that Ref/Im f is typically $0.1 \to 0.2$. i.e. $|\mathrm{Re} f|^2$ term is .01 to .04 of $d\sigma/dt$ and errors in extrapolation or normalization are very important in this method.

(2) Coulomb Interference. This is a much better method. To the basic strong interaction amplitude $A(s,t)$, we must add electromagnetic corrections. Normally these are of $O(\alpha)$ and irrelevant. However there is one place where they are huge. This is small t where Coulomb scattering

$\sim e^2/t$ in

amplitude dominates due to pole at $t=0$. This is comparable to nuclear amplitude for $-t \sim .005$. (See Fig. 2(d) (h) of Physics Letters 59B, 308 (75).) This amplitude is real. Thus measured of $d\sigma/dt$ very near $t=0$ is proportional to

$$|\text{Im } A|^2 + |\underbrace{A_C}_{e^2/t} + \text{Re}A|^2$$

For $-t \sim .005$ we can assume that Re A and Im A - the nuclear terms (which have a scale $\sim (300 \text{ MeV})^2$ are constant. Thus magnitude and t dependence of cross section $d\sigma/dt$ can give Re A (sign and magnitude).

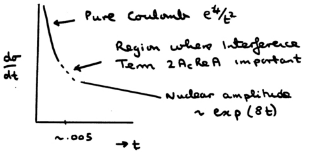

Volume 59B, number 3 PHYSICS LETTERS 10 November 1975

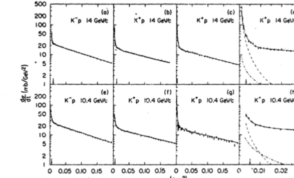

Fig. 2. $K^\pm p$ differential elastic scattering cross sections at 14 GeV/c (a) K^-p elastic, (b) K^+p elastic, (c) K^+p Coulomb, (d) K^+p Coulomb for $t < 0.030$ GeV^2 and at 10.4 GeV/c, (e) K^-p elastic, (f) K^+p elastic, (g) K^+p Coulomb, (h) K^+p elastic for $t < 0.030$ GeV^2. The lines shown are the fits described in the text. The fit starts at a t value indicated by an arrow. In d and h the separate contributions from pure Coulomb (- - -) and interference (-. -.) terms are given.

Table 2

Results of the fits. The errors in ( ) are the possible systematic errors associated with each measurement. The number of degrees of freedom DF is indicated besides the χ^2. The limits of the fitted region are t_{min} and t_{max}.

Momentum (GeV/c)	Ratio of real to imaginary amplitude α	Slope b (GeV^2)	c (GeV^{-4})	χ^2(DF)	t_{min} (GeV^2)	t_{max} (GeV^2)
K^+p						
13.90 Coulomb	− 0.10 ± 0.05 (± 0.01)	6.15 ± 0.15	− 0.5	36(54)	0.003	0.210
14.00 Elastic	− 0.15 ± 0.03 (± 0.02)	6.09 ± 0.07	− 0.5	49(34)	0.010	0.180
10.40 Coulomb	− 0.21 ± 0.12	5.68	0	35(38)	0.001	0.200
10.40 Elastic	− 0.21 ± 0.06 (± 0.02)	5.68 ± 0.10	0	38(30)	0.005	0.200
K^-p						
14.00 Elastic	0.00 ± 0.04 (± 0.03)	8.14 ± 0.07	− 1.3	43(23)	0.010	0.200
10.40 Elastic	0.08 ± 0.04 (± 0.02)	8.20 ± 0.09	− 1.6	41(33)	0.005	0.200

Volume 59B, number 3 PHYSICS LETTERS 10 November 1975

F normalization factor,

α ratio of real to imaginary nuclear amplitude,

b nuclear slope, c curvature,

Q charge of the incident particle,

t momentum transfer in GeV^2,

σ_T total cross section in mb,

$\delta = -[\ln[(b/2 + 5.6)t] + 0.577]/137$ Coulomb phase shift taken from ref. [4].

M_N, M_C, M_I are the multiple scattering terms and can be derived using Moliere's theory [5,6]. In the fitting domain one can derive approximate expressions:

$$M_C = [1 - 5(\theta_s/\theta)^2]^{-4/5}, \qquad M_I = 1 + 2(\theta_s/\theta)^2,$$

$$M_N = 1 - 2.16 \times 10^{-4}\,(\sigma_T^2/b)\,[1 - 0.25\exp(bt/2)],$$

where θ_s is the multiple scattering angle defined in ref. [5]. To account for the experimental resolution itself, we have folded a Gaussian distribution, using the experimentally determined width, over the theoretical expression weighted by our acceptance. At 3 mrad and 14 GeV, this effect increases dN/dt by 17%, but is already negligible at 6 mrad. In doing our calculation, we admitted implicity that there was no strong correlation between angular spread and vertex position spread. If there were a correlation the effect should be small since some of these extra events would lie outside the cut on the Z distribution. The data favor the no-correlation hypothesis and further we see no significant dependence of our result with the Z cut.

The folded theoretical values are then compared to the measurements and a fit is performed allowing b, α and the normalization F to vary. σ_T is taken from ref. [7] and its error is incorporated in the determination of α. Due to limited statistics for the 10.4 GeV/c K^+p Coulomb data, we have constrained the nuclear slope to the value found from the elastic events. Table 2 summarizes our results and fig. 2 shows the $d\sigma/dt$ distributions for 10.4 and 14 GeV/c for K^+p and K^-p scattering together with the fitted curves. For K^+p scattering the results from the separate Coulomb and elastic geometry data samples are in good agreement. Notice that for the Coulomb K^+p data, the fits extend to smaller t values than needed to measure the interference effect. By doing this we do not gain much in accuracy but we are able to check that the corrections are well understood. By varying the low momentum transfer cut off for each fit, we can study the small changes in the results and thus get an estimate of the systematic errors quoted in table 2.

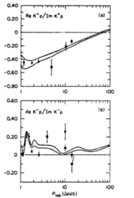

Fig. 3. Comparison of Re ($K^{\pm}p$)/Im($K^{\pm}p$) measurements with dispersion relations predictions [3] (hatched area). All experimental results displayed measure the interference effect.

(a) K^+p measurements: • This experiment, ▲ ref. [12], ▪ ref. [13].
(b) K^-p measurements: • This experiment, ▲ ref. [12], ▪ ref. [14], × ref. [15], ♦ ref. [16].

In the fit, a small t dependence of the slope was included. We used the curvature c obtained from the high statistics elastic data [8]. Also the real part could have a different t slope than the imaginary; however, this has no practical effect on the measurement of the real part because of the very restricted t region of interference: if the real part slope were half that of the imaginary part it would result in only a 1% variation of α.

In fig. 3 we compare our results with the predictions of $t = 0$ dispersion relations [3] including recent data on total cross sections [9]. There is agreement for both

Subtractions

For the case discussed above [f(s) in (10) is A(s,t=0) for elastic scattering] the condition (4), $f(s) \to 0$ as $s \to \infty$, is not satisfied. In fact we will later find that $A(s,t) \sim s^{\alpha(t)}$ as $s \to \infty$ at fixed t; for the case of interest $\alpha(t)$ is the "Pomeranchuk Regge Trajectory" (or Pomeron) and $\alpha(0) = 1$. The behavior $A(s,t=0) \sim s$ corresponds from (9) to constant total cross sections asymptotically. Experimentally there appears to be a gradual rise of σ_{total} with energy but this is only logarithmic (one can show that σ_{total} can rise at most like $\log^2 s$ - the Froissart bound). As (4) is not satisfied, the integrals in (10) do not converge and one must slightly extend the formalism. We use a subtracted dispersion relation which means using for f(s) in (2)

$$f(s) = \frac{A(s,t=0)}{(s - s_0)(u - u_0)} \tag{11}$$

where the choice $s_0 = u_0$ is natural, and clearly now $f(s) \to 0$ as $s \to \infty$. This gives us a result like (10) except that we have not only the dynamical pole (with residue in f(s) of $C'/(s_{pole} - s_0)(u_{pole} - u_0)$ at $s = s_{pole}$ but also poles at $s = s_0$ and $u = u_0$. The residues of these artificial poles are unknown; the result is a two parameter formula for Ref as a function of s. One can use Ref at low energies to find these two parameters and use (10) to predict Ref at higher energies. This procedure is particularly transparent if I choose $s_0 = (m + \mu)^2$, $u_0 = (m+\mu)^2$. Then the subtraction constants residues of artificial poles) are just threshold scattering amplitudes.

One can always choose to use more subtractions than are necessary to ensure convergence of integrals. For instance if I take

$$f(s) = \frac{A(s,t=0)}{(s - s_0)^2(u - u_0)^2} \tag{12}$$

then I will find a four parameter formula for Re A. (The unknown parameters will be the value and derivative of A at $s = s_0$ and $u = u_0$). The integral analogous to (10) will involve

$$\int \frac{\text{Im } A(s',t=0)\ ds'}{(s'-s)(s'-s_0)^2(u'-u_0)^2} \tag{13}$$

and the integrand behaves like $1/s'^4$ as $s' \to \infty$ and is more convergent than the $1/s'^2$ arising in the integral if we had used (11). The extra convergence in (13) may be important because although Im A can be related to total cross section measurements these are naturally only known up to some finite energy and one must extrapolate them to infinite energy in order to evaluate the integrals to infinite s' and u' in (10). Naturally the more convergent integrals following from (12) will be less sensitive to the extrapolation to infinity than those using (11). Thus we have a choice of swopping extra unknown (usually low energy) subtraction constants for unknown high energy behavior. Im A is conventionally extrapolated to infinity using forms suggested by Regge theory. (See our later discussion.)

Resonances in Dispersion Relations

One seemingly distrubing feature of (10) is that we have an explicit pole term for nucleon pole (or any bound state below threshold) but no mention of any resonances. How is this consistent with the obvious symmetry between the nucleon and $\Delta^0(1234)$? The answer is that the latter contributes through the dispersion integral

$$\int \frac{du'\ \text{Im } f(u')}{u'-u} \tag{14}$$

In fact using the form

$$f(u) = \frac{C}{u - m_\Delta^2 + i\Gamma_R\, m_\Delta\, p(u)/p(m_\Delta^2)} \tag{15}$$

(cf (2) in Section VIII.B) for Im f(u') one can show that the result of dispersion integral (14) is approximately

$$\frac{C}{u - m_\Delta^2} \tag{16}$$

at large u ($u - m_\Delta^2 >> \Gamma_R m_\Delta$) - in exact anology to the nuclear pole term. The result (16) is no accident but can be derived. Thus the nucleon pole term comes from the clock-wise integral around the pole location.

Now the Δ pole lives on second sheet gotten by going through u cut and I can exhibit this explicity by moving cut up into

complex plane. Then moving contour C through pole I pick up a pole contribution that is <u>exactly</u> (16) (for $\Gamma << m_\Delta$). I still have a remaining integral but this can be moved a long way from the Δ pole and so there is no reason for the Δ to have any effect on it and indeed (16) is contribution of Δ.

<u>Nearly Singularities</u>

One can write dispersion relations in t at fixed s. Consider the reaction $np \rightarrow pn$ and s fixed at some reasonable value (say not too near threshold and not too high an energy). Then we have a right-hand cut starting at $t = 4\mu^2$ (μ is pion mass, note t channel is $n\bar{p} \rightarrow p\bar{n}$ but lowest threshold is 2π and <u>not</u> $\bar{p}n$), a pole at $t = \mu^2$ and a left-hand cut at $u = 4\mu^2$ or $t = 4m^2 - s - 4\mu^2$

(m nucleon mass)

$$f(s\ \text{fixed},t) = \frac{C}{\mu^2 - t} + \int_{4\mu^2}^{\infty} \frac{\text{Im}\ f(t')\ dt'}{t' - t} + \text{left-hand cut} \qquad (17)$$

For small $t \sim 0$ (in physical region) we see that the first term dominates - $1/(\mu^2 - t) \gg 1/(t' - t)$ - especially as in integral Im $f(t')$ vanishes as $t' \to 4\mu^2$ and so mean t' in integral is substantially larger than $4\mu^2$ (integrand will not become large until $t' \sim m_\rho^2$ when ρ resonance enhances integrand as discussed in last section - cf. Eq. (16)). Thus dispersion relations justify the use of Born term - even in a strong interaction problem when all terms are comparable - in a certain kinematic region. The pion pole in (17) is called a nearby singularity. The π is the best example of this because of its small mass - the most sophisticated example being PCAC (partially conserved axial current) theory.

VIII.E. Determination of Singularities of Analytic Functions Represented In Integral Form.

We follow the treatment in chapter 2 of ELOP. We consider

$$f(z) = \int_a^b \frac{dw}{w - z} \tag{1}$$

$$= \log \frac{b - z}{a - z} \tag{2}$$

We see from (2) that f(z) is singular for z = a and z = b and cut from z = a and z = b. The discontinuity across the cut is $2\pi i$. Let us see why this is obvious from (1).

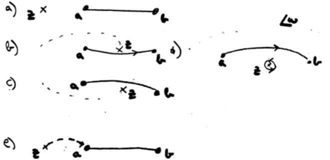

Figures (a) to (e) show various configurations in the complex w plane. In Fig. (a) we show z < a,b when f(z) is clearly well defined. We now analytically continue z to the real axis between w = a and b. The integral is not singular because we can distort the w contour down into complex w plane. Figures (c) and (d) show that f(z) is in fact cut for $a \le z \le b$ because one must distort contours in different ways depending whether z approaches the real axis from above or below. In (d) we see that $f(\mathrm{Re}z + i\varepsilon) - f(\mathrm{Re}z - i\varepsilon)$ is just a contour integral around $w = z$ of $1/w - z$; this gives a $2\pi i$ residue in agreement with evaluation below (2). Finally in Fig. (e) we show that the integral is singular for $z = a$(or b, not shown) because at these end points of the integration one cannot of course distort the w contour. The points $z = a$ and b are typical of a type of singularity called an end point singularity.

The second fundamental type of singularity is illustrated by

$$f(z) = \int_0^1 \frac{dw}{(w - z)(w - a)} \quad , \quad \underline{a > 1} \tag{3}$$

$$= \frac{1}{(z - a)} \log\left[\frac{a(1 - z)}{(1 - a)z}\right] \tag{4}$$

This is again cut between $z = 0$ and 1 and this is only singularity on physical sheet. The analysis of this cut is very similar to that of the integral (1) with $z = 0$ and 1 being end point singularities.

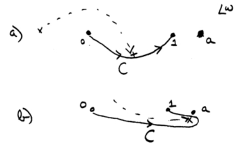

We see above the point z being continued through the cut onto an unphysical sheet. The pole $1/(w - z)$ "pushes" the contour ahead of it. This maintains a well defined integral except $z = a$ when you see contour is trapped between the moving pole $1/(w - z)$ and the fixed pole $1/(w - z)$. This is called a pinch singularity. The nature of singularity can again be discovered by splitting contour C as sketched below

The singularity is contained in circular integral around $w = a$ and has value $2\pi i/(a - z)$ in agreement with evaluation from (4) [the log multiplying $1/(z - a)$ is 0 on physical sheet and $2\pi n i$, n integral on unphysical sheets].

As described in ELOP, one can use this to discuss singularities of Feynman integrals. If one uses the Feynman parameteric form [with integrals $d\alpha_i$ $0 \le \alpha_i \le 1$, $\sum_i \alpha_i = 1$) one gets both end point ($\alpha_i = 0$) and pinch singularities. In momentum space one can only get pinch singularities as the end points are at infinity.

Consider a simple integral

for quark propagator.

$$I \propto \int \frac{d^4k}{(k^2 - m_g^2)((p-k)^2 - m_q^2)} \tag{5}$$

Abstract this as

$$I = \int \frac{dw_i}{S_1 \; S_2} \tag{6}$$

where $S_j(w_i)$ are surfaces and w_i are complex variables. Now clearly we may get a pinch singularity if

$$S_1 = S_2 = 0 \tag{7}$$

but this is not sufficient because the existence of several integration variables allows the contour additional freedom to escape the coalescing singularities. In fact near (7) we have

$$I = \int \frac{dw_i}{\left(\sum_i \eta_i \left.\frac{\partial S_1}{\partial w_i}\right|_0\right)\left(\sum_i \eta_i \left.\frac{\partial S_2}{\partial w_i}\right|_0\right)} \tag{8}$$

with $\eta_i = w_i - w_i^0$

and $S_1(w_i^0) = S_2(w_i^0) = 0$.

Now change variables from w_i to a set that <u>includes</u>

$$\xi_1 = \sum_i \; \eta_i \left.\frac{\partial S_1}{\partial w_i}\right|_0$$

$$\xi_2 = \sum_i \; \eta i \left.\frac{\partial S_2}{\partial w_i}\right|_0 \tag{9}$$

If J is Jacobian we find

$$I = \int \frac{J d\xi_1 \; d\xi_2 \; ..}{\xi_1 \; \xi_2} \tag{10}$$

But now it is clear that I is not singular at all because each integral $d\xi_j$ includes but one singularity and is not pinched at all. The above argument fails if ξ_1 and s_2 are the same and so we deduce that we need as well as (7)

$$\frac{\partial S_1}{\partial w_i} \propto \frac{\partial S_2}{\partial w_i} \tag{11}$$

Now we need one other condition to ensure that the coalescing singularities actually trap the contour, i.e.

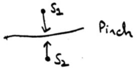

rather than approaching from some side, i.e.

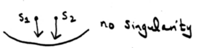

This final condition states that $\frac{\partial S_1}{\partial w_i}$ and $\frac{\partial S_2}{\partial w_i}$ have opposite sign.

We summarize the conditions (7) and (11) as

$$\begin{aligned} &S_1 = S_2 = 0 \\ &\alpha_1 \frac{\partial S_1}{\partial w_i} + \alpha_2 \frac{\partial S_2}{\partial w_i} = 0 \qquad \alpha_1,\ \alpha_2 \text{ positive} \end{aligned} \tag{12}$$

Applying (12) to (5) we find that the propagator is singular for

$$k^2 = m_g^2 \tag{13a}$$

$$(p - k)^2 = m_q^2 \tag{13b}$$

$$\alpha_1 k + \alpha_2(k - p) = 0 \tag{13c}$$

The last equation (13c) says p and k are parallel (as 4 vectors), $p = \gamma k$, γ real.

Putting this in (13b) gives

$$(\gamma - 1)^2 = (m_q/m_g)^2$$

$$\gamma = 1 + m_q/m_g$$

or

$$p^2 = (m_q \pm m_g)^2 \tag{14}$$

which is the "normal" unitarity threshold we stated earlier. The choice $\gamma = 1 - m_q/m_g$, $p^2 = (m_q - m_g)^2$, corresponds to $\alpha_1/\alpha_2 < 0$, i.e. the non-singular situation with both singularities the same side of the contour. $\gamma = 1 + m_q/m_g$. $p = (m_q + m_g)^2$ is a true pinch.

If we now look at a box diagram

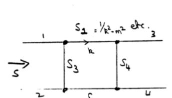

We find a pinch from $S_1 = S_2 = 0$ at $s = (m_1 + m_2)^2$ and a pinch from $S_3 = S_4 = 0$ at $t = (m_1 + m_3)^2$. We can also get more complicated pinch singularities involving more than two $_j$. The condition for any of the singularities can be summarized by the Landau Rules.

$$\alpha_1 S_1 = \alpha_2 S_2 = \alpha_3 S_3 = \alpha_4 S_4 = 0$$

$$\sum_j \alpha_j \frac{\partial S_j}{\partial w_i} = 0 \tag{15}$$

$$\sum_i \alpha_i = 1, \text{ (α_i positive is normally pinch requirement)}$$

where say $\alpha_1 \neq 0$, $\alpha_2 \neq 0$, $\alpha_3 = \alpha_4 = 0$ gives $s = (m_1+m_2)^2$ singularity mentioned above. If $\alpha_i = 0$ it is equivalent (singularity wise) to contracting corresponding propagator to a point, i.e. $\alpha_3 = \alpha_4 = 0$ contracts box diagram to propagator. If α_1, α_2, α_3 and α_4 are all non-zero, then one finds the "Landau Singularities" given in VIII.F ($D = 0$ in Eq. (12)). If three are non-zero and one zero one finds the singularities of the triangle graph discussed at length in ELOP but not present on physical sheet of box diagram.

VIII.F The Mandelstam Representation and His Iteration

We now come to some pretty theory due to Mandelstam which was the cornerstone of the attempts to build a dynamical theory out of analyticity and unitarity. We will explain how this works for potential scattering but failed in practice when applied to quantum field theory. In writing dispersion relations, we will temporarily ignore possible subtracting and take potential scattering to begin with. Then VIII.D (7) with $f(s) = A(s,t)$ for any fixed t becomes

$$A(s,t) = \frac{1}{\pi} \int_{s_1}^{\infty} \frac{ds'}{s' - s} \; \mathrm{Im}\, A(s',t) \tag{1}$$

Now $\mathrm{Im}\, A(s',t) = \frac{1}{2i} \{A(s' + i\epsilon,t) - A(s' - i\epsilon,t)\}$ is an analytic function of t. Thus we can write a dispersion relation in t at fixed s'. Let $\rho(s',t')$ be

$$\mathrm{Disc}_t \frac{1}{2i} \{A(s' + i\epsilon,t') - A(s' - i\epsilon,t')\}$$

$$= -\frac{1}{4} \{A(s' + i\epsilon,t' + i\epsilon) - A(s' + i\epsilon,t' - i\epsilon)\}$$

$$- A(s' - i\epsilon,t' + i\epsilon) + A(s' - i\epsilon,t' - i\epsilon)\} \tag{2}$$

Then we find

$$A(s,t) = \frac{1}{\pi^2} \int_{s_1}^{\infty} \int_{t_1}^{\infty} \frac{\rho(s',t')\, ds'dt'}{(s' - s)(t' - t)} \tag{3}$$

where ρ is called the double spectrum function. We will soon see that ρ is only non-zero in a somewhat smaller region than the naive estimate above. i.e. $s' \geq s_1$, $t' \geq t_1$ (s_1, t_1 are lowest thresholds in s and t channels respectively). If we have poles in s and t channels at $s = s_o$ and $t = t_o$ respectively then one must add to (3)

$$g_s/(s_0 - s) + g_t/(t_0 - t) \tag{4}$$

Note a subtlety: namely the s channel pole appears directly in s dispersion relation (1) but where does t channel pole fit in? It clearly must be of the form (4) because of the symmetry of (3) in $s \leftrightarrow t$. However $g_t/(t_0 - t)$ will not occur in t channel dispersion relation for Im $A(s',t)$ because it has zero s discontinuity. Noting that as a function of s, $g_t/(t_0 - t)$ is a constant we see that it appears in the formalism as a subtraction constant in s dispersion relation.

(3) + (4) is the Mandelstam representation for nonrelativistic scattering. For field theory we must replace (3) by

$$\begin{aligned} A(s,t) = {} & \frac{1}{\pi^2} \int_{s_1}^{\infty} \int_{t_1}^{\infty} \frac{\rho_{st}(s',t')\, ds'dt'}{(s' - s)(t' - t)} \\ & + \frac{1}{\pi^2} \int_{s_1}^{\infty} \int_{u_1}^{\infty} \frac{\rho_{su}(s',u')\, ds'du'}{(s' - s)(u' - u)} \\ & + \frac{1}{\pi^2} \int_{t_1}^{\infty} \int_{u_1}^{\infty} \frac{\rho_{tu}(t',u')\, dt'du'}{(t' - t)(u' - u)} \end{aligned} \tag{3'}$$

with $s' + t' + u' = \Sigma\, m^2$ as usual.

Let us now return to (3) and show how to calculate $\rho(s,t)$. This involves quite a bit of algebra which we will not do in detail. Take the simple elastic scattering case with all particles of mass m. Let q be c.m. momentum. Then unitarity takes the form

$$A_s(i \to f \;:\; s, z_{if})$$

$$= \frac{1}{8\pi^2} \int A(i \to n \;:\; s, z_{in})\, A^*(n \to f \;:\; s, z_{nf})$$

$$\frac{d^3E_5\, d^3E_6}{2\, E_5\, 2E_6} \quad \delta^4(p_1 + p_2 - p_5 - p_6) \tag{5}$$

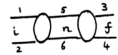

i is initial state, f final state and n intermediate state. 1,2,3,4 are in xz plane and each scattering is specified (in c.m. system) by polar angle θ_{in}, θ_{nf} and θ_{if}. $z_{in} = \cos\theta_{in}$ etc. It is easy enough to calculate the phase space integrals in (5) (as long as one works in c.m. system!) using spherical polar angles θ_{in}, ϕ_{in} to specify direction of n wrt an initial state i along the z direction.

A_s denotes $\frac{1}{2i}\{A(s + i\varepsilon, z) - A(s - i\varepsilon, z)\}$ where $z = 1 + t/2q^2$ is an equivalent variable to t which is used here because it makes unitarity easier. We find (5) can be written

$$A_s(i \to f \;:\; s, z_{if}) = \frac{q}{64\pi^2\sqrt{s}} \int_0^{2\pi} d\phi_{in} \int_{-1}^{+1} dz_{in}$$

$$A(i \to n \;:\; s, z_{in})\, A^*(n \to f \;:\; s, z_{nf}) \tag{6}$$

Now we transform variables from ϕ_{in} natural from phase space to z_{nf}. This needs the Jacobian

$$\frac{\partial(z_{in},\phi_{in})}{\partial(z_{in},z_{nf})} = \frac{\theta(-D(z_{in},z_{nf},z_{if}))}{(-D)^{1/2}(z_{in},z_{nf},z_{if})} \tag{7}$$

with

$$D(\alpha,\beta,\gamma) = \alpha^2 + \beta^2 + \gamma^2 - 1 - 2\alpha\beta\gamma \tag{8}$$

Thus we finally reach the useful form of unitarity

$$A_s(i \to f \ : \ s,z_{if}) = \frac{q}{32\pi^2\sqrt{s}} \int dz_{in}\, dz_{nf}\, \frac{\theta(-D)}{(-D)^{1/2}}$$

$$A(i \to n \ : \ s,z_{in})\, A^*(n \to f \ : \ s,z_{nf}) \tag{9}$$

For some purposes it is convenient to write this as integrals wrt t not z and this is trivial as $dz = dt/2q^2$. The next step is to write dispersion relations in t_{in}, t_{nf} for the amplitudes $A(i \to n)\, A^*(n \to f)$. This exhibits explicitly the z_{in} and z_{nf} dependence as $1/(z_{in} - z'_{in})$ etc. and the integrals $dz_{in}\, dz_{nf}$ can be done analytically. The result is

$$A_s(i \to f \ : \ s,z_{if}) = \frac{q}{16\pi^3\sqrt{s}} \int \frac{dt'_{in}}{2q^2}\, \frac{dt'_{nf}}{2q^2}$$

$$A_t(i \to n \ : \ s,z'_{in} = 1 + t'_{in}/2q^2) A^*(n \to f \ : \ s,z'_{nf}$$

$$= 1 + t'_{nf}/2q^2)$$

$$\frac{1}{D^{1/2}(z_{if},z'_{in},z'_{nf})} \log\left\{\frac{z'_{in}z'_{nf} - z_{if} + D^{1/2}}{z'_{in}z'_{nf} - z_{if} - D^{1/2}}\right\} \tag{10}$$

Note in the above z'_{in}, z'_{nf} are both > 1 while the physical cosine $z_{if} < 1$. Then automatically $D^{1/2}(z_{if}, z'_{in}, z'_{nf}) > 0$. The equation for $D(z_{if}, z'_{in}, '_{nf}) = 0$ regarded a function of z_{if} for fixed z'_{in}, z'_{nf}, is a quadratic for z_{if} with two solutions, $z_{if} = z_{if}^{<}$ and $z_{if}^{>}$ (with naturally $z_{if}^{>} > z_{if}^{<}$). We can now finally achieve our goal and take the $t_{if} = t$ (or $\propto z_{if}$) discontinuity on both sides of (10); a tricky analysis shows that the right hand side is singular for $z_{if} > z_{if}^{>}$ and we get

$$\rho_{st} = \frac{1}{32\pi^2 q^3 \sqrt{s}} \int \frac{dt'_{if}\, dt'_{nf}\, \theta(D)}{D^{1/2}}$$

$$A_t(s, t'_{in})\, A_t(s, t'_{nf}) \tag{11}$$

where

$$D = \frac{1}{4q^4} \{t^2 + t_{in}^2 + t_{nf}^2 - 2tt_{in} - 2tt_{nf} - 2t_{in}t_{nf} - tt_{in}t_{nf}/q^2\}$$

$$= \frac{1}{4q^4} \{E(t, t_{in}, t_{nf}) - tt_{in}t_{nf}/q^2\} \tag{12}$$

where asymptotic (as $q \to \infty$) form

$$E(t, t_{in}, t_{nf}) = [\sqrt{t} - \sqrt{t_{in}} - \sqrt{t_{nf}}][\sqrt{t} - \sqrt{t_{in}} + \sqrt{t_{nf}}]$$
$$[\sqrt{t} + \sqrt{t_{in}} - \sqrt{t_{nf}}][\sqrt{t} + \sqrt{t_{in}} + \sqrt{t_{nf}}] \tag{13}$$

Given that $\theta(D)$ in (11) corresponds to $t(z_{in})$ being larger than bigger of two solutions of $D = 0$, we see that for all q we must have:

$$\sqrt{t} \geq \sqrt{t_{in}} + \sqrt{t_{nf}} \tag{14}$$

Now let us apply the above formalism to the box diagram

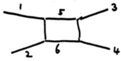

Unitarity gives the correct value of ρ_{st} for this diagram as one uses the Born term $g_t/(t_0 - t)$ to calculate A_t on right hand side.

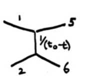

This term clearly corresponds to

$$A_t = \pi g_t \, \delta(t_0 - t) \tag{15}$$

with
$$\rho_{st} = \frac{1}{32q^3\sqrt{s}} \quad \theta(D)/D^{1/2}[t,t_0t_0] \tag{16}$$

ρ is non-zero for the region $D \geq 0$. The boundary $D = 0$ clearly satisfies

$$\sqrt{t} = 2\sqrt{t_0} \qquad \text{as } q \to \infty$$
$$t \to \infty \qquad \text{as } q \to 0$$

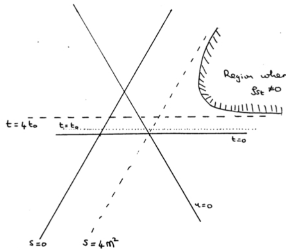

We can now form

$$A_t(t,s) = \frac{g_t}{t_0 - t} + \frac{1}{\pi} \int \frac{\rho_{st}(s',t)\, ds'}{s' - s} \qquad (17)$$

where the second term only contributes for $t \geq 4\, t_0$. We can now use (17), as an improvement over (15), in (11) to calculate ρ_{st} to higher order in g_t. Mandelstam's important observation was that this is not just a (divergent) strong interaction perturbation theory. Rather we see that the second term in (17) (the $0(g_t^2)$ term in A_t) only contributes to ρ in (11) for $\sqrt{t} \geq \sqrt{t_0} + \sqrt{4t_0}$ i.e. $t \geq 3t_0$. Thus the formula (16), and hence (17), is <u>exact</u> for $2\sqrt{t_0} \leq \sqrt{t} \leq 3\sqrt{t_0}$.

Use of (17) in (11) gives a ρ_{st} exact for $\sqrt{t} \leq 4\sqrt{t_0}$. Clearly the method can be iterated in a well defined and exact fashion to give ρ_{st} for all t and to all orders in g_t. In potential theory, the input $g_t/(t_0 - t)$ Born term corresponds to specification of potential. (This is correct for a Yukawa potential - naturally you can input other potentials - they can always be decomposed as a sum (integral) over Yukawa forms). Normally one is interested in bound states of theory. These do not appear directly because they correspond to forms

$$A(s,t) = g_s/(s_0 - s) \tag{18}$$

for such an s-wave potential and such a form has zero t channel discontinuity, i.e. will not contrubute to A_t which is determined directly by ρ_{st} from (17). We will later find that for large t, A_t behaves like $t^{\alpha(s)}$ where $\alpha(s)$ is a Regge trajectory with

$$\alpha(s_0) = 0 \tag{19}$$

corresponding to the bound state (18).

The picture below shows how s_0 can be found by extrapolation (or use of a dispersion relation in s for $\alpha(s)$ - itself an analytic function with a cut for $s > 4m^2$) of value found by fit of t dependence of $\rho(s,t)$ for $s > 4m^2$.

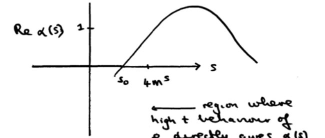

This will become clearer when we do Regge theory later.

Chew (and Mandelstam) hoped that this technique would be used for quantum field theory. There are two extra difficulties compared to potential scattering case.

(1) There are 3 double spectral functions and left hand cuts in the dispersion relations.

(2) The above assumes single channel two body unitarity. In quantum field theory, one has an infinity of 2 and >2 body channels.

The difficulty (2) is the essential problem. The high multiplicity intermediate states are critical and there is no practical method to include them. Chew tried to parameterize them but this did not work. Thus foundered this (and similar) attempts to calculate strong interactions from analyticity and unitarity alone.

VIII.G. Regge Theory

This was originally introduced in potential scattering by Regge (see a very nice book by V. de Alfaro and T. Regge, "Potential Scattering" - North Holland, 1965). However, the extension to relativistic QFT is quite straightforward. We consider the crossed process $a + \bar{d} \to c + \bar{b}$ (i.e., $\bar{p}p \to \pi^+\pi^-$ in our standard example) where t is the energy variable; s and u are momentum transfers. We write down a partial wave expansion

$$A^{(t)}(t,s) = \sum_{\ell}(2\ell+1)P_\ell(\cos\theta_t)a_\ell(t) \tag{1}$$

t channel process [$A^{(t)}(t,s)$ is analytic continuation of $A^{(s)}(s,t)$].

The partial wave amplitudes are a function of t; the s and u dependence is contained in $\cos\theta_t$. Let us take equal mass scattering; the complication of unequal masses is important in detail but unimportant in general concept. In this case, $\cos\theta_t$ can be simply written:

$$\cos\theta_t = 1 + \frac{s}{2p^2}.$$

Here the t channel cms momentum p is just $1/2\sqrt{t-4m^2}$ in the equal mass case. Now this series converges for $-1 \le \cos\theta_t \le 1$ but it is easy to show that it diverges as soon as $\cos\theta_t$ gets much bigger than 1. We wish to analytically continue this outside t channel physical region where it is defined and converges.

Suppose $a_\ell(t)$ can be continued to complex ℓ. Then we can write

↓ takes care of residue of pole in $\sin\pi\ell$

$$A^{(t)}(t,s) = -\frac{1}{2i}\int_C (2\ell+1)a_\ell(t)\,\frac{P_\ell(-\cos\theta_t)}{\sin\pi\ell}\,d\ell \qquad (2)$$

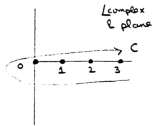

as is obvious from Cauchy's theorem.

Now we move C to run parallel to imaginary axis and move it as far to the left as possible.

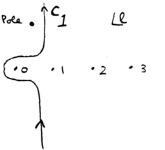

The circle at infinity vanishes as it is damped by $1/\sin\pi\ell$ which behaves like $\exp[-\pi \mathrm{Im}\,\ell]$. Now this will be legitimate as long as $a_\ell(t)P_\ell(-\cos\theta_t)$ behaves well enough at ∞. We will return to this point later.

The integral along C_1 is useful in the limit $\cos\theta_t = z_t \to \infty$. Thus $P_\ell(-z_t) \sim z_t^\ell$ as $z_t \to \infty$. As I move C_1 to the left, I decrease $\mathrm{Re}\ell$ and hence $A^{(t)}(t,s)$ gets a better and better bound as $z_t \to \infty$. I can move the contour to the left until I hit a singularity of $a_\ell(t)$ [$P_\ell(-\cos\theta_t)$ is an entire function of ℓ while additional poles of $\sin\pi\ell$ are, in fact, uninteresting - they are canceled]. The simplest singularity - which is all that occurs in potential scattering - is a pole. The position $\ell = \alpha(t)$ of pole in $a_\ell(t)$ will, in general, be a function of t. The contribution of a pole - which is called a Regge pole after T. Regge who found them - is:

$$a_\ell(t) = \beta(t)/[\ell-\alpha(t)] \tag{3}$$

in $a_\ell(t)$ and from Cauchy's theorem this gives the scattering amplitude:

$$A^{(t)}(t,s) = -\pi[2\alpha(t)+1]\beta(t)\ \frac{P_{\alpha(t)}[-z_t]}{\sin\pi\alpha(t)}. \tag{4}$$

Subtracting this pole term from $a_\ell(t)$ we can continue contour further to the left. The contribution of this remaining contour is $\leqslant z_t^{\mathrm{Re}\ell_{max}}$ ($\leftarrow$ largest real part on contour) as $z_t \to \infty$. Thus the Regge pole term dominates as $z_t \to \infty$.

In general one may expect

a) Several Regge poles. In this case, the pole which is furthest to the right, i.e., has the largest real part, will dominate as $z_t \to \infty$. The contribution of other Regge poles is still significant, of course, and describes approach to asymptotic limit given by leading trajectory.

b) Poles and <u>cuts</u>. There are no cuts in potential scattering (except for some pathological potentials). But in relativistic theories there are cuts.

This is the main problem with Regge theory. A pole is characterized by two numbers $-\alpha, \beta(t)$ for each t. A cut is parameterized by a function for each t - the cut discontinuity.

c) Note that one believes that - as long as suitable technical precautions are taken - the contour can be taken to $\mathrm{Re}\,\ell = -\infty$. Thus amplitude can be expressed as a sum of Regge pole and cut contributions. Note this sum is correctly interpreted as an asymptotic series as $z_t \to \infty$, i.e., series does not converge at fixed z_t as number terms included increase; rather it converges as $z_t \to \infty$ for a fixed number of terms.

Regge poles have one other aspect that is very important. Namely when t is such that $\alpha(t)$ = an integer, then the pole in $a_\ell(t)$ coincides with a physical value of ℓ

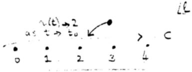

The contour C is "pinched" (in language of VIII.E) and as there we get a singularity in the analytic function $A^{(t)}(t,s)$ represented by integral (2). [Note that a Regge pole is always a singularity in the ℓ plane but $A^{(t)}(t,s)$ is normally nonsingular as it is just a residue of this pole.] We can see what is going on by taking limit $\alpha(t) \to$ integer in (4).

We only have to be careful in $\sin\pi\alpha(t)$ term. Suppose

$$\alpha(t) = \alpha(t_o) + (t-t_o)\alpha' \tag{5}$$

is a Taylor expansion near t_o. Then $\sin\pi\alpha(t_o) = 0$ if $\alpha(t_o)$ is an integer and

$$\sin\pi\alpha(t) = \sin\pi\alpha(t_o) + \pi\underbrace{\cos\pi\alpha(t_o)}_{(-1)^{\alpha(t_o)}}(t-t_o) \; . \tag{6}$$

Therefore $$A^{(t)}(t,s) = -(2\alpha(t)+1)\,\frac{\beta(t)}{t-t_o}\,P_{\alpha(t_o)}(Z_t) \tag{7}$$

i.e., this is just a contribution of a pole in $\underline{t}$ (not ℓ this time!). The pole has spin $\alpha(t_o)$

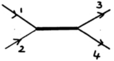

so Regge poles correspond to real live particles at t values where $\alpha(t)$ takes integral values. Regge poles are illustrated in Fig. 7 of the picture book and in Fig. VIIIG.1.

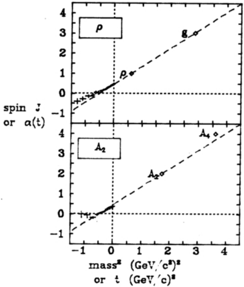

Fig. VIIIG.1: The ρ and A_2 Trajectories

Note that for reasons we will soon describe in QFT, only states differing by 2 in ℓ lie on the same trajectory. Such states have identical internal quantum numbers - including the same parity - just the spin changes by 2. We give some examples below:

J = 1	3			
ρ	g	I = 1	G+	P-
ω	$\omega(1670)$	I = 0	G-	P-
J = 2	4			
A_2	A_4	I = 1	G-	P+
f	h	I = 0	G+	P+

The remarkable feature of all Regge trajectories found so far is that they are all approximately straight lines in the J - m^2 plane with a universal slope $\alpha' \sim 0.9\ \mathrm{GeV}^{-2}$

$$\alpha = \alpha_o + \alpha' t.$$

The straight lines link

$$\left.\begin{array}{ll} \text{spins} & 0 - 2 - 4 - 6 \ldots \\ \text{or} & 1 - 3 - 5 \ldots \end{array}\right\} \text{mesons}$$

$$\left.\begin{array}{ll} & 1/2 - 5/2 - 9/2 \ldots \\ \text{or} & 3/2 - 7/2 - 11/2 \ldots \end{array}\right\} \text{baryons}$$

In potential scattering Regge trajectories do not look like this and tend asymptotically to -1 as $t \to +$ or $- \infty$. (This follows at once because Born term dominates in the limit $t \to \pm\infty$.)

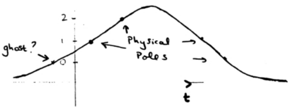

The ghost marked above will have zero residue in a sensible theory!

One point I should remind you of is that for $t >$ threshold ($4m^2$ in equal mass case), the points t_o (where poles are) are at complex values $t_o = (m-i\Gamma/2)^2$. Correspondingly if $\alpha(t_o) = 2$, say, then α is real when t_o is complex but α(real argument) is, in fact, complex. Thus plots we have made are Reα for real values of t_o. There is also an Imα for real t. As $\Gamma << m$, Im$\alpha << 1$ and the imaginary part does not make any essential difference.

Now we turn to the other aspect of Regge poles. Namely they control behavior as $z_t \to \infty$ at fixed t. In potential scattering this has no physical interpretation, but in QFT the analytic continuation principle (crossing) leads to a beautiful interpretation illustrated below

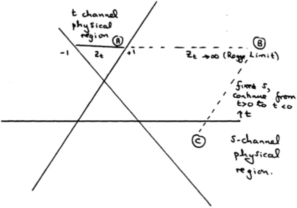

The classical (potential theory) Regge limit concerns the behavior under the continuation from A to B above. B is always unphysical but if we continue in t from B from C we find the limit $s \to \infty$ for the s-channel process.

Putting $P_\ell(-z_t) \sim s^\ell$ times a function of t as $s \to \infty$ in (4), we find the basic predictions

$$A^{(s)}(s,t) = F(t)s^{\alpha(t)} \tag{8}$$

$$\frac{d\sigma}{dt} = G(t)s^{2\alpha(t)-2} \tag{9}$$

where F and G are functions of t which can be related to "kinematic" factors and the residue $\beta(t)$ of the Regge pole defined in (4). Regge theory is discussed in Figures 12 and 13 of the Picture Book.

We test this theory as shown in Fig. 13(b) of the picture book. We use a log log plot of $s^2\, d\sigma/dt$ versus s. The result should be a straight line - and the slope is just $2\alpha(t)$. The critical test is that when we find an $\alpha(t)$ for $t < 0$ by studying $d\sigma/dt$ that is consistent for that found for $t > 0$ from the particles. Amazingly this is true as illustrated in Fig. VIIIG.1 and surveyed in detail by Fox and Quigg, Annual Review of Nuclear Science 23, 219 (1973). We now consider the possible Regge trajectories where we will see that the interesting trajectories are those from $L = 0$ and 1 $q\bar{q}$ states. The higher L quark states are just Regge recurrences of these. Let us illustrate this.

For $q\bar{q}$ spin $S = 0$, we have (L is conventional $q\bar{q}$ relative orbital angular momentum)

$L = 0$ $J = 0$ π, η, K trajectories - naturally we have SU(3) nonets of trajectories,

but $L = 2$ $J = 2$ states have not been seen yet experimentally. All trajectories so far seen have a slope $\alpha' \sim 0.9$ GeV^2, so we predict that the $\ell = 2$ partner of π has a mass^2 = $m_\pi^2 + (\Delta J{=}2)/0.9 \sim 2.2$ GeV^2.

$L = 1$ $J = 1$ B, etc. Again recurrences are unknown. Note that π and B are "exchange degenerate": namely in potential theory with an exchange force (see later) π and B would be on the same trajectory. $m_B^2 - m_\pi^2$ is too large for this limit to be a good approximation experimentally for canonical 0.9 GeV^{-1} slope.

Now we turn to quark spin $S = 1$ states. For general L we get $J = L - 1$, L, $L + 1$. Note that Regge poles are in J <u>not</u> L, and $d\sigma/dt \sim s^{2J-2}$, <u>not</u> s^{2L-2}. Thus as trajectories with highest J dominate as $s \to \infty$, the series $J = L + 1$ will be most important. These are (see table on p. 49)

$S = 1 \quad L = 0 \quad J = 1 \quad \rho$ nonet

with recurrence

$S = 1 \quad L = 2 \quad J = 3 \quad$ g nonet

and $\quad S = 1 \quad L = 1 \quad J = 2 \quad A_2$, f.. nonet

with recurrence

$S = 1 \quad L = 3 \quad J = 4 \quad A_4$, h nonet.

The less important trajectories from the series $J = L$, $J = L - 1$ are

$S = 1 \quad L = 1 \quad J = 0 \quad \delta$ nonet $\quad$ } no recurrences known

$S = 1 \quad L = 1 \quad J = 1 \quad A_1$ nonet

$S = 1 \quad L = 2 \quad J = 1$ } spawn new trajectories as

$\qquad\qquad\quad J = 2$

$L = 0$ does not contribute to this series.

It appears that not many mesons on each Regge trajectory are known. However, the situation is much better for the baryons (see Fig. 7 of picture book) for experimental reasons we discussed in V.B.5.

Note that not all the Regge trajectories (e.g., $S = 1$, $L = 1$, $J = 2$) have the (naively) expected spin 0 members. These omissions predicted by the quark model are confirmed experimentally. [The pole given by (7) is "killed" by an explicit factor $\alpha(t)$ in $\beta(t)$.]

Regge trajectories are associated with a given set of conserved quantum numbers. One discovers what Regge trajectories contribute to a particular reaction by just asking if the associated particle poles contribute.

The importance of the reaction of $\pi^- p \to \pi^o n$ is that only ρ exchange contributes and so one has a clean test of (9). Most other reactions which have measured have contributions from several exchanges. For instance, $pp \to pp$ allows

$$\rho,\ \omega,\ f,\ A_2,\ \pi,\ \eta,\ A_1,\ B\ ..\ \text{exchanges.}$$

All these trajectories have $\alpha(0) \leqslant 0.5$ (look at masses and spins).

$\therefore$ $d\sigma/dt \sim s^{2\alpha-2}$ falls at least as fast as $1/s$. This is in complete contradiction with $pp \to pp$ experimental data where $d\sigma/dt \sim$ constant with increasing s at fixed t. This implies existence of a singularity with $\alpha = 1$. This is called the Pomeron or Pomeronchuk trajectory (picture books - Figs. 21 $\to$ 23). It has no known particle associated with it. It is also known experimentally that the slope $\alpha'_{\mathcal{P}}(0)$ of the Pomeron is small - not 0.9 but perhaps 0.2 and possibly even zero. It is also possible that Pomeron is not a pole in ℓ plane but a cut going from $-\infty$ to 1. The Pomeron trajectory dominates all elastic or diffractive (no quantum number exchange) processes. Its quantum numbers are the same as those of "vacuum"

$(-1)^J P = +$ [the product $(-1)^J$ x parity is the only meaningful parity for a Regge trajectory]

$I = 0 \quad C = +$ etc.

Let us comment at this stage that (7) is true for Feynman diagram Born terms involving a single particle exchange

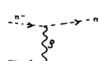

where we use the usual Feynman Rules for a spin 1 particle interacting with a spin 0 and 1/2 particles. This theory has $\alpha = 1$ and predicts $d\sigma/dt \sim$ constant independent of s in complete contradiction with experiment

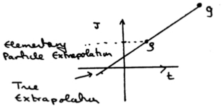

In Regge theory, the contributions of all the particles on the trajectory add up to give the observed $\alpha(t)$ where for the crossed physical region $\alpha(t)$ is less than the spin of any individual particle on trajectory $\alpha_0 + \alpha' t$ [clearly there is a lot of cancellation]. A fixed spin independent of t is characteristic of an elementary particle. The hadrons are not elementary and so our "effective" field theory of ρ, π and nucleons gave the wrong answer. There <u>are</u> elementary spin 1 particles in QCD - the gluons - but these can't contribute to $\pi^- p \to \pi^0 n$ because of the necessary flavor exchange. However, it <u>is</u> reasonable to associate the Pomeron (at least at large t) with multiple (≥ 2 to get color correct) gluon exchange.

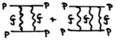

This interpretation suggests that "glueballs" (bound states involving gluons but no quarks) are the particles to be expected on the Pomeron trajectory.

Signature

Let us now discuss why Regge trajectories only give rise to particles separated by 2 and not 1 in the angular momentum plane. In potential scattering (without an exchange potential) they are separated by 1. The reason is rather technical.

We wish to define $a_\ell(t)$ for complex ℓ so that it converges as $\mathrm{Im}\,\ell \to \infty$ and so that we can, in fact, unfold the contour in (2). Now:

$$a_\ell(t) = \frac{1}{2}\int_{-1}^{+1} A^{(t)}(t,s)P_\ell(z^{(t)})dz^{(t)}. \tag{10}$$

We write a fixed t dispersion relation in s,u or equivalently $\cos\theta_t = z^{(t)}$

$$A^{(t)}(t,s) \equiv A^{(t)}(t,z^{(t)}) = \frac{1}{\pi}\int_{z_s}^{\infty} \frac{A_s^{(t)}(t,z^{(t)\prime})}{z^{(t)\prime}-z^{(t)}}\,dz^{(t)\prime} + \frac{1}{\pi}\int_{z_u}^{\infty} \frac{A_u^{(t)}(t,-z^{(t)\prime})}{-z^{(t)\prime}-z^{(t)}}\,dz^{(t)\prime} \tag{11}$$

where z_s and z_u are > 1.

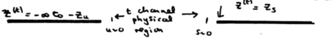

Now you can look up

$$Q_\ell(z^{(t)\prime}) = \frac{1}{2}\int_{-1}^{+1} \frac{dz^{(t)}P_\ell(z^{(t)})}{z^{(t)\prime}-z^{(t)}} \tag{12}$$

$$\therefore\ a_\ell(t) = \frac{1}{\pi}\int_{z_s}^{\infty} A_s^{(t)}(t,z^{(t)'})Q_\ell(z^{(t)'})dz^{(t)'} \tag{13a}$$

$$+\frac{1}{\pi}\int_{z_u}^{\infty} A_u^{(t)}(t,-z^{(t)'})Q_\ell(-z^{(t)'})dz^{(t)'}. \tag{13b}$$

Note that (10) is only equivalent to (13) for integer ℓ. They correspond to <u>different</u> continuations of a_ℓ to complex ℓ. There is clearly an ambiguity in this continuation of the form

$$a_\ell \to a_\ell + b(\ell)\sin\pi\ell \tag{14}$$

where $b(\ell)$ is regular for integral ℓ.

Now (13a) is splendid as

$$Q_\ell(z) \underset{|\ell|\to\infty}{\to} \ell^{-1/2}\exp[-(\ell+1/2)\log[z+(z^2-1)^{1/2}]] \tag{15}$$

but (13b) is awful as

$$Q_\ell(-z_t') = (-1)^{\ell+1}Q_\ell(z_t'>1)$$
$$\downarrow$$
$$-e^{i\pi\ell} \tag{16}$$

and $e^{i\pi\ell}$ diverges.

Note in potential scattering only the right hand cut contribution (12) exists and (13b) is absent. We solve the problem given by (13b) by defining

$$a_\ell^{\pm}(t) = \frac{1}{\pi}\int_{z_s}^{\infty} A_s^{(t)}(t,z^{(t)'})Q_\ell(z^{(t)'})dz^{(t)'} \pm \frac{1}{\pi}\int_{z_u}^{\infty} A_u(t,-z^{(t)'})Q_\ell(z^{(t)'})dz^{(t)'}. \tag{17}$$

Now both $a_\ell^\pm$ are always convergent as $\ell \to \infty$ and

$$a_\ell^+ = a_\ell \quad \ell \text{ even}, \quad a_\ell^- = a_\ell \quad \ell \text{ odd} \tag{18}$$

or
$$2a_\ell = a_\ell^+(1+(-1)^\ell) + a_\ell^-(1-(-1)^\ell). \tag{19}$$

Regge poles occur in a_ℓ^+ or a_ℓ^- with separate poles in each. They obviously only give physical particles (i.e., those occurring in a_ℓ) for $\Delta\ell = 2, 4 \ldots$ as we mentioned before. The above factors give rise to characteristic

$$(1+\tau e^{-i\pi\ell}) \tag{20}$$

factor in Regge pole contribution. Here τ is signature of trajectory, e.g.,

$\tau = +$ Pomeron contributes to a_ℓ^+

$\tau = -$ ρ contributes to a_ℓ^-.

The exchange degeneracy limit is the left hand cut $A_u = 0$ where $a_\ell^+ \equiv a_\ell^-$ and + and - signature trajectories are degenerate. It seems to be a good approximation for the $\rho - A_2 - g - A_4$ and SU_3 related $\bar{q}q$ trajectories. In
L=0 1 2 3
potential scattering (without an exchange force), there is no left hand cut and so trajectories create particles for $\Delta J = 1$ and not $\Delta J = 2$ necessary when $A_u \neq 0$.

Regge Poles in Field Theory

Regge poles are generated by summing ladder diagrams as is illustrated below for $\pi\pi$ scattering

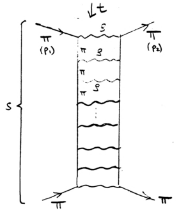

$\pi\pi$ Scattering

which have exactly the same structure as potential scattering - especially if one uses a Yukawa potential which has the same $(1/(t-\mu^2))$ form as a single particle Born term in a field theory.

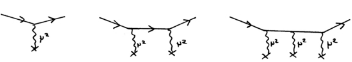

Potential Scattering

(Turn this through 90° to get comparison with QFT ladder above.)

Note that one finds Regge poles by summing ladders in limit

fixed external masses

fixed t

$s \to \infty$.

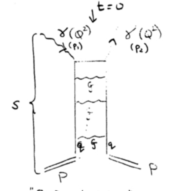

"QCD Ladders"

The typical logarithmic behavior of QCD at high Q^2 also comes from ladder diagrams (pictured above) where

external masses $Q^2 \to \infty$

fixed $t = 0$

$s \to \infty$ such that s/Q^2 fixed.

The theory applicable to the high Q^2 or Regge limits is essentially the same with angular momentum ℓ in the Regge case being replaced with a moment (or Mellin transform) index n in QCD. Mathematically the difference is that in the Regge case $t = (p_1-p_2)^2$ is generally nonzero [p_i marked in diagrams above] and little group of $p_1 - p_2$ is SU(2) with ℓ labeling its representations. In QCD, $p_1 = p_2$ (t=0) and little group is full homogenous

Lorentz group with representations labeled by n. The QCD limit turns into the Regge limit when $s/Q^2 \to \infty$ or $x_{BJ} \to 0$

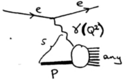

$$\frac{s-m^2}{Q^2} = \frac{1}{x_{BJ}}$$

(m = mass of proton)

In field theory, one has many more complicated diagrams than those used in the ladders, e.g.,

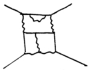

This might affect structure in the ℓ-plane, i.e., it will change residues/positions of poles and cuts but the ℓ plane still retains its value because angular momentum is a conserved quantum number.

Let us consider how poles are built up taking spin 0 internal and external particles. We could get this in $\pi\pi$ scattering by replacing spin 1 ρ by spin 0^+ ε resonance; we will go through analysis for potential theory case

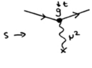

The Born diagram above is

$$A(s,t) = \frac{g}{\mu^2 - t} \tag{21}$$

$$\sim \frac{g}{t} \text{ as } t \to \infty \text{ at fixed s.} \tag{22}$$

Comparing this to the Regge form, $t^{\alpha(s)}$, we see $\alpha(s) = -1$ from this diagram. In potential theory the Born term dominates as $s \to \infty$ and so we find that all trajectories in potential theory $\to -1$ (or lower $-2, -3...$ in ℓ plane) as $s \to \pm\infty$. We can use the Mandelstam iteration discussed in VIII.F to show how things go in higher orders. From VIII.F (16), we see that as $t \to \infty$, the double spectral function

$$\rho(s,t) \to h(s)/t \text{ as } t \to \infty \tag{23}$$

where the function

$$h(s) = \frac{1}{16q\sqrt{s}} \tag{24}$$

$h(s)$ is $O(1/s)$ as $s \to \infty$.

Using a fixed t dispersion relation on (23) we see that A_t is also $O(1/t)$ as $t \to \infty$. Clearly the function $\frac{\log t}{t}$ has (t-channel) discontinuity $1/t$ and so

$$A(s,t) \sim \ln t/t \tag{25}$$

as $t \to \infty$. Iterating this, we find that the n-th Born term has the behavior

$$\frac{g(gk(s))^{n-1}}{n!} \frac{\ell n^{n-1}(t)}{t} \tag{26}$$

which sums to $gt^{\alpha(s)}$ where

$$\alpha(s) = -1 + gk(s) \tag{27}$$

and $k(s) \sim 1/s$ as $s \to \infty$. The behavior (26) is the "leading log" approximation familiar from QCD. Nonleading log terms such as

$$\frac{g(gk(s))^{n-1}}{n!} \frac{\ell n^{m-1}(t)}{t}, \; m < n \tag{28}$$

will lead to a power series expansion for $\alpha(s)$

$$\alpha(s) = -1 + gk(s) + g^2 \ldots . \tag{29}$$

and corrections to the residue

$$\beta(s) = g + O(g^2/s) + \ldots \quad . \tag{30}$$

The "leading log" approximation is good if the coupling constant g (or rather "effective coupling" gk(s)) is small but $g \, \ell n \, t \sim 1$. The corresponding approximation in high Q^2 QCD is reasonable (as g is indeed small) but it is not very reliable in our Regge pole application as Q^2 is small and the QCD coupling constant is large.

(29) and (30) show the structure already described for potential scattering with $\alpha(s) \to -1$ in the region where the "effective coupling constant" $gk(s)$ is small (whatever size of g).

In QCD we expect the coupling constant to be small when both s and t are large; equivalently this is the fixed angle (or fixed t/s) limit as $s \to \infty$. As above we expect the Born term to be dominant there and α to tend to an integer (half integer for baryon exchange). In QCD the Born terms are always box diagrams and not single (as colored) particle exchange.

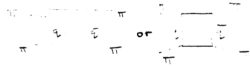

Now as another application of VIII.F, we consider the result of combining two general amplitudes

A_o = 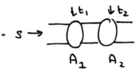

where for dubious reasons, we have swopped s and t compared to our discussion above, where $A_i(s,t) \sim g_i(t)s^{\alpha_i(t)}$. Using VIII.F (6) with $dz \sim dt/ds$, we see that

$$A_o(s,t) \sim s^{\alpha_1(t_1)+\alpha_2(t_2)-1} \tag{31}$$

where t_1, t_2 are integrated over the allowed kinematic region - as given in VIII.F (9). For $t = 0$, $t_1 = t_2$ runs from 0 to $-\infty$; for $t \neq 0$ the region is much more complicated. We now apply (31) to the π-π scattering box diagram above. We see that each $\alpha_i = 1/2$ and so the resultant box has $\alpha = 1/2 + 1/2 - 1 = 0$, i.e., because the exchanged quarks have spin 1/2 we have promoted the usual limit $\alpha = 0 + 0 - 1 = -1$ (cf. (29)) to 0. In elastic processes one can have diagrams like

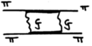

with limit $\alpha = 1 + 1 - 1 = 1$.

So the QCD weak coupling limit corresponds to $\alpha = 0$ or 1 and not the -1 seen in potential scattering. Experimentally there is evidence for $\alpha(\text{large } t) \sim 1$ from elastic pp scattering at the ISR. However, the $q\bar{q}$ $\alpha = 0$ value expected in quantum number exchange processes has not been tested because the cross sections have not measured well as they are much smaller than those in elastic scattering.

Regge Cuts

Summing ladders gives Regge poles, i.e.,

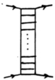

and generally no cuts - which is simple analytic structure in ℓ plane found in potential scattering.

Unfortunately, it was soon realized that one could combine Regge poles

as 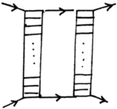 or 

Putting the intermediate particles "on shell", i.e,

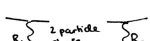

One can use (31) to find behavior of "Regge" box diagram

$$A_o \sim \int dt_1 dt_2 \, s^{\alpha_1(t_1)+\alpha_2(t_2)-1} . \tag{32}$$

Now in (31) α_i were integers and then the resultant behavior of A_o is still proportional to an integer power of s. However, if we put Regge poles $\alpha_i(t_i)$ in (32), we get a completely different behavior, e.g., if

$$\alpha_i(t_i) = \alpha' t_i + \alpha_{oi}$$

and we take $t = 0$, then the region of integration in (32) is just $0 \geq t_1 = t_2 \geq -\infty$ and so (32) can be written as

$$A_o \sim \int_{-\infty}^{\alpha_{o1}+\alpha_{o2}-1} f(\ell) s^{\ell} d\ell \tag{33}$$

i.e., A_o has a <u>cut</u> in ℓ plane stretching from $-\infty$ to $\alpha_{o1} + \alpha_{o2} - 1$.

For arbitrary t, the kinematic region for the t_i is more complicated but clearly one will still find cuts.

If α_1 and α_2 are $q\bar{q}$ Regge poles then at least for $t = 0$, the tip of cut $\ell = \alpha_{o1} + \alpha_{o2} - 1$ is lower than pole as $\alpha_{oi} \leq 1/2$.

Unfortunately, taking for example $\pi^- p \to \pi^o n$, one can form box diagrams involving one exchanged leg as the Pomeron

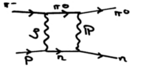

ℙ = Pomeron

Taking (approximately valid) limit $\alpha_{\mathcal{P}}(t) \equiv 1$ we see that the tip of cut in above box goes precisely up to

$$\alpha_{cut} = \alpha_\rho(0) + 1 - 1 = \alpha_\rho(0) \tag{34}$$

i.e., cut is asymptotically as important as the pole! This is the curse of Regge theory. One can never escape the cuts (above we took $t = 0$, for $t < 0$ the situation is worse - the cut is above pole). Unfortunately, the discontinuity ($f(\ell)$ in (33)) across cuts cannot either be calculated [the Regge box diagram is only typical and not the only way of getting cuts] or parameterized and discovered from realistic experiments. Some reactions (such as $\pi^- p \to \pi^0 n$) have (empirically) a small cut discontinuity and one can see the simple Regge pole contribution. However, there are no general rules for calculating the sizes of the discontinuity - the "approximation" (model) of using the Regge boxes (with intermediate particles on shell) to calculate the cuts is called the absorption model. However, this model is almost certainly unjustified. For instance, Mandelstam showed that whereas the diagram (where $R_{1,2}$ are simple ladders) has a Regge cut when e and f are placed on shell, it does not when it is calculated as a full Feynman diagram with e,f as propagators.

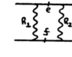

Unfortunately, Mandelstam found a set of more complicated diagrams for which the cut is not canceled! The box with e,f on shell gives the correct cut position but the wrong discontinuity.

Triple Regge Theory

This is an extension of Regge theory to inclusive reactions

$$ab \to cX. \tag{35}$$

It is illustrated for $pp \to pX$ in Fig. 29 of the picture book. When $t = (p_a - p_c)^2$ is small and $s = (p_a + p_b)^2$ is large (35) is described by

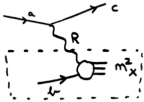

an exchange of a Regge pole R.

Clearly the fully inclusive (35) is gotten when the dashed box in the figure above is given by Rb total cross-section. If you are worried that Reggeon particle cross sections mean anything, just go to poles on R trajectory - define particle cross sections there - and analytically continue in Reggeon spin ℓ.

The Rb total cross section (proportional to imaginary part of forward Rb elastic scattering amplitude) is itself given by Regge pole R' exchange when the c.m. energy squared m_X^2 for the Rb process is large. So triple Regge theory given diagrams like

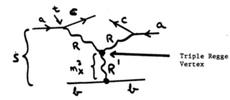

which describe (35) when t is small and s, m_X^2 are large.

The theory predicts

$$\frac{d\sigma}{dtdx} \propto \frac{(1-x)^{\alpha'-2\alpha(t)}}{s^{1-\alpha'}} \tag{36}$$

(α' is intercept at momentum transfer 0 or Reggeon R', $\alpha(t)$ is trajectory of R) or for $\alpha' = 1$ (the Pomeron) one finds the energy independent inclusive cross section

$$\frac{d\sigma}{dtdx} \propto (1-x)^{1-2\alpha(t)}. \tag{37}$$

This theory was successfully tested in our experiment described in Section VI.G.

VIII.H. Duality, Finite Energy Sum Rules, The Veneziano Model

Finite Energy Sum Rules (abbreviated FESR) are a combination of Regge theory and dispersion relation ideas (see Masataka, Fukugita and Igi, Physics Reports 31C, 237 (1977)). Consider the relation VIII.D (7) using $f(s) = \nu^N A(s,t)$, $\nu = (s-u)/2$ {N an integer and A our amplitude}. Let us assume that f(s) vanishes faster than s^{-1} as $s \to \infty$. In the Regge pole language this means that $N+\alpha_{max}(t) < -1$. Then for large s we can replace $1/s_p-s$ and $1/s'-s$ by just $1/-s$.

$$\therefore f(s) = -\frac{1}{s}\{c' + \frac{1}{\pi}\int_{s_1}^{\infty} ds'\mathrm{Im}f(s') - \frac{1}{\pi}\int_{u_1}^{\infty} du'\mathrm{Im}f(u')\} \qquad (1)$$

with (a formal) error of order $1/s^2$.

But by assumption there is no 1/s term in f(s). Thus the coefficient of 1/s must vanish:

$$c' + \frac{1}{\pi}\int_{s_1}^{\infty} ds'\mathrm{Im}f(s') - \frac{1}{\pi}\int_{u_1}^{\infty} du'\mathrm{Im}f(u') = 0. \qquad (2)$$

(2) is called a superconvergence relation (SCR) and is the forerunner of FESRs. We will evaluate the SCR by

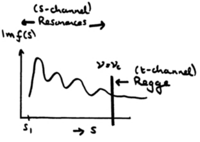

using resonances at low values of s and the Regge pole expansion for large s. Using a Regge pole contribution for $\nu > \nu_c$, i.e.,

$$A \sim \frac{\nu^{\alpha}\beta(t)[1+\tau e^{-i\pi\alpha}]}{-\sin\pi\alpha} \int_{\nu=\nu_c}^{\infty} ds'\nu'^{N} \mathrm{Im}A_s \tag{3}$$

We find that
$$\int_{\nu_c}^{\infty} ds'(=d\nu')\nu'^{N}\beta(t)\tau\nu'^{\alpha}$$
$$= -\frac{\nu_c^{N+\alpha+1}}{N+\alpha+1}\,\beta(t)\tau. \tag{4}$$

We now calculate the Regge pole contribution for the left hand cut (u channel) contribution $\nu < -\nu_c$

In the Analytic Continuation from P to Q, we get $\nu \to |\nu|e^{i\pi}$ and so the amplitude

$$A \text{ (evaluated for } -|\nu| \text{ at Q)} = \frac{|\nu|^{\alpha}\beta(t)}{-\sin\pi\alpha}\,[e^{i\pi\alpha}+\tau]. \tag{5}$$

Now go from Q to R using hermitean analyticity

$$A(z) = A^{*}(z^{*}) \tag{6}$$

$$A \text{ (evaluated at } -|\nu| \text{ at R)} = \frac{|\nu|^{\alpha}\beta(t)}{-\sin\pi\alpha}\,[1+\tau e^{-i\pi\alpha}].\tau \qquad (7)$$

i.e., A (evaluated at R) = τA (evaluated at P)

i.e.,
$$\mathrm{Im}A_u = \tau\,\mathrm{Im}A_s. \qquad (8)$$

Thus the total Regge pole contribution to (2) is

$$\int_{\nu=\nu_c}^{\infty} ds'\nu'^N \mathrm{Im}A_s - \int_{-\nu=\nu_c}^{\infty} du'\nu'^N \mathrm{Im}A_u = -[1-(-1)^N\tau]\,\frac{\nu_c^{N+\alpha+1}}{N+\alpha+1}\,\beta(t)\tau \qquad (9)$$

and (2) becomes

$$c' + \frac{1}{\pi}\int_{s_1}^{s(\nu=\nu_c)} ds'\,\mathrm{Im}f(s') - \frac{1}{\pi}\int_{u_1}^{u(\nu=-\nu_c)} du'\,\mathrm{Im}f(u') = \tau\beta(t)[1-(-1)^N\tau]\,\frac{\nu_c^{N+\alpha(t)+1}}{N+\alpha(t)+1}. \qquad (10)$$

This is the basic FESR. It relates the integral over the low energy (resonance) amplitude to the Regge contribution. Now we have only derived it on the assumption that $\alpha < -1$ for this was the condition for the SCR (2) to be true. Now whereas SCR was nonsense for $\alpha > -1$ the above relation is at least well defined for $\alpha > -1$: it may, of course, be incorrect! In hadron scattering amplitudes, it is, however, correct even if $\alpha > -1$. [It is not correct for Compton scattering $\gamma N \to \gamma N$ though.]

A simple way to see that it may be true is to use analyticity in the fixed variable t. Maybe $\alpha(t_1) > -1$. However, suppose there exists a t_2 with $\alpha(t_2) < -1$. Then for $t = t_2$ the FESR (10) is exact; now analytically continue from $t = t_2$ to $t = t_1$. Both sides of the FESR are analytic in t and we derive the FESR for all t.

Even if $\alpha(t)$ is never < 1, in real life we only need to find one parameter (e.g., the strong interaction coupling constant) which we can continue analytically until $\alpha(t_1) < -1$.

A more straightforward method is to consider the $\int \nu^N f(s)ds$ over the contour below

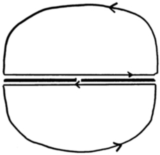

This is part of the problem sets. We should also, of course, say that in FESR (10) we sum over all trajectories on the right hand side.

It is instructive to consider the FESR for $\pi^+\pi^o \to \pi^o\pi^+$ at fixed $t \sim 0$. The only Regge trajectory is the

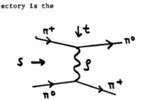

and the FESR relates this to the imaginary part of the low energy s and u channel amplitudes

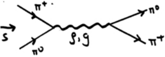

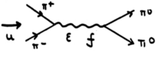

If we are brave, we can apply the FESR with a value of ν_c corresponding to an s value between the ρ and f resonances. Then the s and u channel low energy amplitudes only get contributions from ρ and ε and the former dominates (due to $(2\ell+1)$ factor in partial wave expansion $A = \Sigma(2\ell+1)a_\ell P_\ell(\cos\theta_s)$). One can also enhance the ρ over the ε contribution by taking $t > 0$ when $\cos\theta_s > 1$ and $P_1(\cos\theta_s) = \cos\theta_s$ for ρ is enhanced over $P_o(\cos\theta_u) = 1$ for ε.

Thus the FESR implies

function (s channel ρ amplitude) $\approx$ function (t channel ρ amplitude). (11)

It is clearly an approximate relation but as described by Collins (p. 217), it gives reasonable results. Thus taking $t = m_\rho^2$, the FESR (10) gives

$$\alpha_\rho' = \frac{3m_\rho^2 - 4m_\pi^2}{\nu_c^2} . \tag{12}$$

Noting $m_\rho^2 = 0.5\ \mathrm{GeV}^2$ and $m_f^2 = 1.5$, it is reasonable to take $s_c = 1\ \mathrm{GeV}^2$ or

$$\nu_c = \frac{(s-u)_c}{2}$$

$$= s_c + \frac{[t-4m_\pi^2]}{2}$$

$$\sim 1.25 \text{ GeV}^2 \text{ for } t = m_\rho^2$$

Thus (12) predicts

$$\therefore \quad \alpha_\rho' \sim 1.5/1.25^2 \sim 1 \text{ GeV}^{-2} \tag{13}$$

in good agreement with the empirical determinations of α' (either from slope in ρ-g plot <u>or</u> $\pi^- p \to \pi^0 n$ scattering data - see slope in Fig. VIII.G.1. We have commented that all (known) Regge poles have a slope ~ 0.9 GeV^{-2}).

A relation like (11) is an example of a "bootstrap" relation which was popularized by Chew at Berkeley but is now considered less important than a few years ago. Thus a t channel exchange can be likened unto a force (cf. electromagnetic force between e and p is t channel exchange

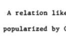

) while s channel diagram is a bound state (created by a force), e.g., the Δ is a bound state of π and N. Thus (11) relates "ρ as bound

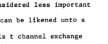

state" to "ρ as force". This is the bootstrap principle. There is no difference between the forces and the bound states.

All the hadrons are forces that create themselves as bound states. Further they are bound states of themselves, e.g.,

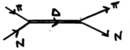

Δ bound state of πN

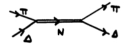

N bound state of πΔ.

Whereas one aspect of this principle is still believed - "namely none of the observed hadrons are more fundamental than any other" (Nuclear democracy) it is, of course, now considered most fruitful to regard hadrons as bound states of quarks and gluons. Hadrons can be regarded as bound states of each other but it is not a dynamical picture with great predictive power.

Now we will discuss an interesting principle called duality. We consider the FESR (10) in another qualitative way (introduced by Dolen, Horn and Schmid while at Caltech). For convenience take a reaction like $\pi^+\pi^0 \to \pi^+\pi^0$ or $\pi^-p \to \pi^0 n$ where the s and u channels are identical (they cancel for one choice of $(-1)^N$, and add for the other). The FESR reads (on including particle poles in s channel contribution as a delta function in the integral)

$$\frac{2}{\pi}\int_{\substack{\text{lowest pole}\\ \text{or threshold}}}^{s(\nu=\nu_c)} \mathrm{Im} f(s')\,ds' \quad : \quad \text{s channel contribution}$$

$$= \sum_{\text{poles}} \tau\beta(t)[1-(-1)^N\tau]\,\frac{\nu_c^{N+\alpha+1}}{N+\alpha+1} \quad : \quad \text{t channel contribution. (14)}$$

The above relation is exact for all ν_c as long as I sum over all the poles (and cuts) in t-channel contribution. If ν_c is large, the "leading" pole(s) (i.e., ones with largest α) will dominate

$$[\nu_c^{N+\alpha_1+1}/\nu_c^{N+\alpha_2+1} = \nu_c^{\alpha_1-\alpha_2} \to 0 \text{ if } \alpha_1 > \alpha_2 \text{ for } \nu_c \to \infty].$$

After the above rigorous remarks, we apply (14) for modest (or indeed rather small) ν_c, but still put only the leading poles in the t-channel contribution. Then (14) is only approximate but we will treat it as an equality!

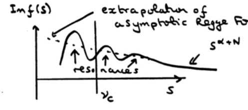

The qualitative message of (14) is:

$$\int^{\nu_c} \text{Imf}(s')ds' \text{ - use s-channel resonance contribution}$$

$$= \int_{\nu_c}^{\infty} \text{Imf}(s')ds' \text{ - use leading t-channel Regge pole contribution.} \quad (15)$$

Now let's consider (approximate) equality (15) as I vary ν_c. Take the difference between the relation (15) for two different ν_c values

$$\int_{s_1(\nu=\nu_{c1})}^{s_2(\nu=\nu_{c2})} ds'\,\mathrm{Im}f(s') = \tau\beta(t)\{1-(-1)^N\tau\}\,\frac{[\nu_{c2}^{N+\alpha+1}-\nu_{c1}^{N+\alpha+1}]}{N+\alpha+1}\,. \qquad (16)$$

This is the origin of duality. The integral over resonance contributions is identical to integral over Regge pole terms. The resonance contribution varies rapidly over an energy scale of order .1 GeV (resonance width) and this variation is not reproduced by Regge term. Rather the Regge term averages the resonance contribution.

This averaging is content of duality. One particular consequence is that amplitude is not given by adding Regge pole and resonance contributions; rather the resonance terms are already included in the Regge terms. This you may consider as another example of the bootstrap principle.

The Veneziano model is a very interesting example of duality. We will write it in a form appropriate for the reaction $\pi^+\pi^- \to \pi^+\pi^-$ (Collins, p. 222-229).

$$A(s,t) = \frac{g\Gamma(1-\alpha(s))\Gamma(1-\alpha(t))}{\Gamma(1-\alpha(s))-\alpha(t))} \tag{17}$$

where $\alpha_s = \alpha_{os} + \alpha' s$

$$\alpha_t = \alpha_{ot} + \alpha' t$$

and slopes α' are identical. The necessity for the slopes to be equal is not immediately obvious. In order to get definite signature it can be shown to be necessary (i.e., st and ut Veneziano forms will only give signature to a t-channel pole if slopes equal in s and u-channel). The intercepts α_{os}, α_{ot} need not be equal.

The amplitude (17) has several interesting properties:

(1) Regge Asymptotic Behavior

Consider t fixed and $s \to \infty$. From Abramovitz and Stegun, we find

$$\Gamma(az+b) \sim \sqrt{2\pi}\, e^{-az}(az)^{az+b-1/2}.$$

Thus $\frac{\Gamma(1-\alpha(s))}{\Gamma(1-\alpha(s)-\alpha(t))} \sim (-\alpha(s))^{\alpha(t)}$

also $\Gamma(1-\alpha(t)) = \frac{\pi}{\Gamma(\alpha(t))\sin\pi\alpha(t)}$

$$\therefore \quad A(s,t) \to \frac{g\pi(-\alpha' s)^{\alpha(t)}}{\Gamma(\alpha(t))\sin\pi\alpha(t)} \text{ as } s \to \infty \text{ at fixed t.} \tag{18}$$

This is the standard Regge behavior with a particular form $\frac{g\pi}{\Gamma(\alpha(t))}$ for the pole residue in the angular momentum plane. We can see from this the expected poles at $\sin\pi\alpha(t) = 0$. Note how the explicit factor $1/\Gamma(\alpha(t))$ kills all the (unphysical) poles for $\alpha(t) \leq 0$.

(ii) Particle Poles

The gamma function has poles when its argument is zero or a negative integer. Thus we see that the amplitude A(s,t) given in (17) has no cuts in complex s,t plane but just a succession of poles. These occur when

$$1 - \alpha(s) = -n \qquad n = 0, 1, 2$$

i.e., $$\alpha(s) = 1 + n$$

or $$1 - \alpha(t) = -m \qquad m = 0, 1, 2$$

$$\alpha(t) = 1 + m$$

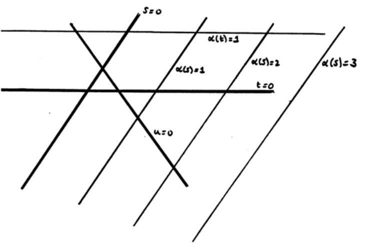

Note there are no poles in u in (17). This is appropriate for $\pi^+\pi^- \to \pi^+\pi^-$ where s and t channels are $\pi^+\pi^- \to \pi^+\pi^-$ but u channel is $\pi^+\pi^+ \to \pi^+\pi^+$ which has no known poles (from $q\bar{q}$ bound states).

This is a reasonable place to discuss exchange degeneracy. (EXD) showed in VIII.G that in a relativistic theory, Regge poles only gave rise to particles with J values that differ by 2. + signature poles gave even J poles; - signature poles gave odd J poles. For $\pi^+\pi^- \to \pi^+\pi^-$ we have (in s or t channel) the - signature ρ and + signature f as dominant poles. These dominate both asymptotic behavior and low lying resonance structure of $\pi^+\pi^- \to \pi^+\pi^-$. Our Veneziano model has given us but a single trajectory with particles at every J value. It has given rise to both the ρ and f trajectories but they are exactly exchange degenerate, i.e.,

$$\alpha_\rho(t) \equiv \alpha_f(t) \tag{19}$$

and residues are also equal. In fact, (19) is not bad experimentally. The reason for the exchange degeneracy is the lack of u channel resonances. Thus (considering t channel Regge trajectories), the necessity to introduce signature was the existence of a left hand cut for $A^{(t)}(t,s)$. The cuts in the Veneziano model are represented by an (infinite) sum of delta function at α(s or t) = integer. The poles from $\alpha(s)$ = integer give a right hand cut to $A^{(t)}(t,s)$ but there are no u channel poles to give a left hand cut. To the extent that the cuts in A are dominated by $q\bar{q}$, qqq resonances we see that this result is more general than the Veneziano model (17)

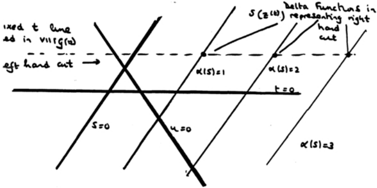

Again exchange degeneracy is more general than the reaction $\pi^+\pi^- \to \pi^+\pi^-$; essentially one finds it whenever one of three channels related by crossing has no resonances; this corresponds to cases when the channel has quantum numbers forbidden by quark model for mesons or baryons. Examples are:

$\pi^+\pi^+ \to \pi^+\pi^+$	$I = 2$
$K^+\pi^+ \to K^+\pi^+$	$S = 1 \quad I = 3/2$
$K^+p \to K^+p$	$S = 1$ baryon.

By looking at enough channels one can show that

$\tau+$	$\tau-$	
f, A_2	ρ, ω	are exchange degenerates
K^*_{1420}	K^*_{890}	are exchange degenerates
f'_{1540}	ϕ	are exchange degenerates

and a similar analysis can be done for the trajectories corresponding to other $q\bar{q}$ quantum numbers. Exchange degeneracy relates the $q\bar{q}$ trajectories starting at L = 0 and 1 with other quantum numbers (spin S and flavor) identical.

(iii) Daughters

Let us return to the Veneziano form (17). The residue of the pole at $\alpha(s) = 1$ is proportional to

$$\frac{\Gamma(1-\alpha(t))}{\Gamma(-\alpha(t))} = -\alpha(t) \text{ as } \Gamma(z) = (z-1)\Gamma(z-1). \tag{20}$$

This is linear in t and can be expressed as a sum of

$$P_o \text{ and } P_1(\cos\theta) \qquad \{\cos\theta = 1+t/2q_s^2\}$$

with coefficients that depend on value of s (= particle mass squared m^2) where $\alpha(s) = 1$. Thus pole at $\alpha(s) = 1$ does not give just J = 1 but a mixture of J = 0 and 1.

Actually this is quite interesting because there is a spin 0 particle (albeit broad and of uncertain mass) - the ε - at about the ρ mass that is a candidate for this prediction from the Veneziano form. (In particle tables, ε is given a large mass but it is consistent with ρ mass given its large width.)

The Regge trajectory structure of Veneziano model is

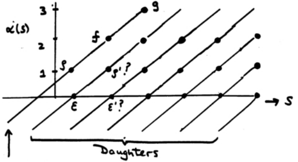

Leading Trajectory

One can show that all theories must have daughters that satisfy

$$\alpha_{d_n}(o) = \alpha(0) - n \qquad (21)$$

↑ integer

↑ s=0 intercept of nth daughter

↑ s=0 intercept of leading trajectory

The fact that daughters are parallel to the leading trajectory for all s is a special feature of the Veneziano form. In the quark model, daughters are radial excitations.

If one inspects the Veneziano form, one can see "why" daughters are necessary. At $\alpha(s) = N$ (any integer) one needs the sum over resonances to be large for small t but small for small u (as there are no u channel poles to exchange). A single resonance of definite J is symmetric on $\cos\theta \to -\cos\theta$ ($t \leftrightarrow u$) and so can never give this behavior.

(iv) Duality

The Veneziano formula is "dual." Namely the same formula exhibits the s and t channel poles. As mentioned when we discussed FESRs, one cannot simply add s-channel resonances to t channel Regge exchange. Although this had been realized before, the Veneziano formula gives an explicit illustration of the general ideas.

(v) Unitarity

The formula has a serious problem; namely α is purely real and all poles are on real axis. This is impossible as the cross section would be infinite. It can only be an approximation to the real world. One must add imaginary parts to the trajectory function to give resonances a width (see discussion before VIII.G (eq. 8). Unfortunately there is no simple way to give α(s or t) an imaginary part that preserves nice features of Veneziano form. For instance, the residue at $\alpha(s) = 1$ was $-\alpha(t)$. If $\alpha(t)$ had an imaginary part (this corresponds to a singularity in $\alpha(t)$ as a function of t at $t = 4m^2$), the residue could never be just linear in t and so $\alpha(s) = 1$ "particle" would have an infinite number of spins.

The fact that the structure in the Veneziano formula is qualitatively akin to nature, suggests that a "narrow resonance" approximation ($\mathrm{Im}\alpha(t) \equiv 0$) may be reasonable as an initial picture of the strong interactions (at low $p_\perp$).

Two Component Duality

We have seen a picture of the strong interactions where s and t channel Regge poles are dual to each other. In the $\pi^+\pi^- \to \pi^+\pi^-$ example, this picture led to a purely real amplitude for $\pi^+\pi^+ \to \pi^+\pi^+$. This corresponded to the lack of resonances in this channel. For $\pi^+\pi^+ \to \pi^+\pi^+$ a real amplitude is, in fact, a good picture at low energies. However, we know one Regge pole - the Pomeron - that

a) Has a purely imaginary amplitude [consider $\frac{1+e^{-i\pi\alpha}}{\sin\pi\alpha}$ as $\alpha \to 1$].

b) Contributes equally to $\pi^+\pi^+ \to \pi^+\pi^+$ and $\pi^+\pi^- \to \pi^+\pi^-$. It certainly isn't much smaller in former case.

c) Has, so far, no known particles on it.

It would be reasonable to suppose that the Pomeron is not in the above picture. This leads to the two component duality picture.

The $q\bar{q}$, qqq states form Regge trajectories that are dual to each other. Namely one can write down a FESR (10) with only $q\bar{q}$ (ρ, A_2 ..) Regge poles on the right hand side and only the same resonances on the left hand side. Note these resonances get more and more dense as $s \to \infty$ and so even though cross-sections are getting smooth as $s \to \infty$, this does not mean there are no resonances. It means that there are so many resonances that they blur together to give a smooth cross-section.

The Pomeron can be used on the right hand side of a FESR but then on the left hand side one includes everything except the $q\bar{q}$, qqq resonances, i.e., one includes "background." So two component duality is

Reggeons $\leftrightarrow$ resonances

Pomeron $\leftrightarrow$ background.

(One often terms all poles with normal slope ($\alpha'\sim 0.9$) Reggeons to distinguish them from the Pomeron - although the latter is, of course, a Regge singularity - it may not be a pole.)

Theoreticians working on the "dual resonance model" (a field theory where the Veneziano model is a Born term and one has "ordinary" Feynman rules with, for instance, Reggeons replacing particles) hope that the Pomeron and "background" will emerge as unitarity corrections (Regge box diagrams) to the Veneziano model.

VIII.I. Low $p_\perp$ Physics

Let me give you a very quick idea of the typical high energy interaction. This is touched on in picture book, page 2.

At low energies ($p_{lab} \leq 5$ GeV/c), the cross section is dominated by 2 body or quasi 2 body final states (quasi means one or more of the "bodies" is a resonance), e.g.,

$$\pi^+ p \to \pi^+ p$$

$$\left.\begin{array}{l} \pi^+ p \to \pi^o \Delta^{++} \\ \pi^+ p \to \rho^o p \end{array}\right\} \quad \text{actually, of course, a } \pi^+\pi^o p \text{ final state, etc.}$$

$$\pi^+ p \to \rho^o \Delta^{++}$$

These two body processes are controlled by Regge poles and cuts. Thus as p_{lab} increases all the 2 body processes, except those with Pomeron exchange, fall with energy like $s^{2\alpha-2}$ with Regge trajectory $\alpha \leq 1/2$ ($= \alpha_\rho(0)$, $\alpha_f(0)$, etc.), i.e., at least as fast as 1/s. Thus as σ_{tot} is approximately constant, we see that 2 body non-Pomeron exchange reactions comprise a smaller and smaller part of the total cross section. We can divide (the nonvanishing asymptotic) cross section into two pieces

a) Diffraction: These are two body and low multiplicity final states governed by Pomeron exchange. This component comprises about 20% of the total cross-section. There are several parts:

i) Elastic

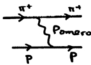

This part is about half the diffractive cross section (i.e., ~ 10% of total cross section).

ii) Diffraction of Excitation Target (p in example)

Here N^* is a nucleon resonance which must have the same internal quantum numbers as the proton (e.g., isospin strangeness, etc.). The spin J can differ but there is some prejudice (not strongly supported experimentally or theoretically) that $(-1)^J P$ (P = parity) should be the same for p and N^*. One has seen experimentally $N^* = N^*_{1470}$ ("Roper" resonance), N^*_{1520} ($J = 3/2^-$) and N^*_{1688} ($J = 5/2^+$). The cross section to produce a given N^* is ~ 5% of the elastic cross section i).

iii) Diffraction Excitation of Beam (π^+ in example)

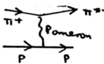

Here the meson resonances $\pi^* = A_1$ and A_2 have been seen. Note that low mass diffractive excitation is confused by the so called Deck effect. This involves elastic scattering of a virtual pion, e.g.,

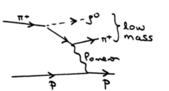

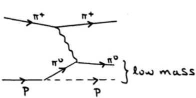

This produces a mass spectrum peaked near threshold; this "kinematic" lump confuses interpretation of the A_1^+ ($\rightarrow \pi^+\rho^0$) and N^{*+}_{1470} ($\rightarrow p\pi^0$ in example) excitation.

Note that the observation of the diffractive production of the A_2 (with $(-1)^J P = +$ whereas pion is $(-1)^J P = -$) shows that the Pomeron can change the value of $(-1)^J P$.

iv) Double Diffraction

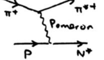

This is rather small both experimentally and theoretically - one can estimate it using factorization which assumes - probably incorrectly - that the Pomeron is a simple pole. Factorization gives

$$\sigma(\text{double diffraction}) = \sigma^2\ (\text{single diffraction, ii), iii) above}) \div \sigma\ (\text{elastic})$$

v) High Mass Diffraction Excitation

The final class of diffraction is:

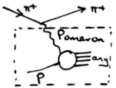

Summed over all particles; the dashed box is Pomeron proton total cross-section. This is quite big and is described by triple Regge formalism which we discussed in VIII.G. v) becomes ii) as the mass of the "any" decreases to the resonance region. There is also an analogous meson excitation.

b) The rest of the cross section (non-Pomeron)

The remainder (~ 80%) of the cross section consists of multiparticle processes. The majority of produced particles are pions. Two key features of π production are:

i) Low $p_\perp$. The transverse momentum is small. A typical formula is

$$E \frac{d^3\sigma}{d^3p} \propto \exp(-6\ p_\perp \text{ in GeV}) \text{ or } \langle p_\perp \rangle \sim .3 \text{ GeV}. \quad (1)$$

The mean $p_\perp$ reflects the size of hadrons. $p_\perp$ is conjugate to transverse size of proton. $p_\perp$ = .3 GeV corresponds to size b ≃ .2/.3 fermi.

ii) The mean multiplicity of produced pions is logarithmically increasing with energy. Roughly

$$\langle n_{all} \rangle \sim 3 \text{ logs + constants}. \quad (2)$$

The logarithmic increase corresponds to a nonzero limit of $Ed^3\sigma/dp$ as p_z (in c.m.) $\to 0$. This gives a cloud of π's with small momentum in c.m.s. (Feynman first understood this). To explore this, let us introduce a new variable called rapidity

$$y = \frac{1}{2}\log\left(\frac{E+p_z}{E-p_z}\right) \text{ or if } E^2 - p_z^2 = m^2 + p_\perp^2 = m_\perp^2 \quad \text{"transverse mass}^2\text{"} \tag{2a}$$

$$= \log((E+p_z)/m_\perp). \tag{2b}$$

Rapidity has a useful feature that under a boost σ in z directions when

$$(E+p_z) \to e^{\sigma}(E+p_z)$$
$$(E-p_z) \to e^{-\sigma}(E-p_z) \tag{3}$$

we get a simple particle independent translation:

$$y \to y + \sigma \tag{4}$$

i.e., in frames that differ by z boosts (e.g., c.m. compared to lab) rapidities differ by a constant that is the same for all particles. We will use rapidity defined in c.m. system when $y_{c.m.} = 0$ is middle value corresponding to $p_z = 0$. The allowed range in y is

$$\log(\sqrt{s}/2m_\perp) \geq |y_{c.m.}| \tag{5}$$

or dropping constants

$$|y_{c.m.}| \le \frac{1}{2}\log(s). \tag{6}$$

Now we can write

$$E\,\frac{d^3\sigma}{d^3p} = \frac{d\sigma}{\pi dyd(p_\perp^2)} \tag{7}$$

as $\qquad dp_z/E = dy$

and $$d^2(p) = dp_x dp_y = p_\perp dp_\perp d\phi = \pi d(p_\perp^2) \tag{8}$$

if $$E\,\frac{d^3\sigma}{d^3p} \sim (\text{constant} = A)\exp(-6p_\perp). \tag{9}$$

Then total multiplicity* is

$$\frac{1}{\sigma}\int_{-\log\sqrt{s}}^{\log\sqrt{s}} dyd(p_\perp^2)\,\frac{d\sigma}{dyd(p_\perp^2)} = \frac{A}{\sigma}\,[\int d(p_\perp^2)\exp(-6p_\perp)]\log s,$$

i.e., it has a logarithmic s dependence as claimed earlier.

* Note $\frac{d\sigma}{dyd(p_\perp^2)}$ is an <u>inclusive</u> cross section: it gets an entry for each particle in each event so that one has the sum rule

$$\sigma_{tot}\langle n\rangle = \int dyd(p_\perp^2)\,\frac{d\sigma}{dyd(p_\perp^2)}\,. \tag{10}$$

iii) One can understand the data on n particle production in terms of an uncorrelated production model. Suppose that the cross section to produce n particles, σ_n, is (the Poisson distribution)

$$\sigma_n = A s^{-\gamma} \frac{\lambda^n}{n!} (\log s)^n \tag{11}$$

coupling constant

identical particles

from integration over n rapidities (with limited $p_\perp$, one has a one dimensional phase space for each produced particle). One gets such a cross section either from "Multiperipheral Model" e.g., (see book by Horn and Zachariasen)

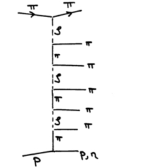

or "Field-Feynman" quark cascade model

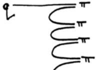

In each case, the links are independent.

Summing σ_n given by (11), one finds a total cross section

$$\sigma_{tot} = As^{-\gamma} e^{\lambda \log s} \tag{12}$$

and so a constant total cross-section implies $\gamma = \lambda$. The mean multiplicity $\langle n \rangle$ is given by

$$\langle n \rangle = \frac{\sum_n n\sigma_n}{\sigma_{tot}} = \frac{1}{\sigma_{tot}} \frac{\lambda \partial}{\partial \lambda} \left(\sum_n \sigma_n\right)$$

$$= \lambda \log s. \tag{13}$$

Thus we get the expected logarithmic multiplicity and the coefficient of log s is just the probability λ to spit off another particle, e.g., in multiperipheral example:

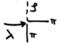

Note for fixed n, σ tends to 0 like $s^{-\gamma}$ so that the constant total cross section is achieved by low multiplicities decreasing and higher multiplicities increasing with s.

From (11), we find

$$\frac{d(\sigma_n)}{d(\log s)} = 0 \text{ at } n = \lambda \log s$$

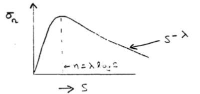

This independent emission model is quite realistic as long as one includes production of full range of particles, i.e., π, ρ, ω, ..., including resonances {reader: think of simple test that distinguishes resonance from single π production - noting there are so many resonances/combinatorial effects that resonances cannot easily be seen in mass spectrum}.

iv) Relation to quarks and gluons (QCD)

There is no known (to be correct) way of describing low $p_\perp$ scattering in QCD. Rather one must wait until one gets to high $p_\perp$ when one can apply perturbative techniques

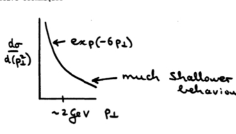

Note that a naive QCD estimate of cross section is $d\sigma/d(p_\perp^2) \sim 1/p_\perp^4$ (at fixed $x_\perp = 2p_\perp/\sqrt{s}$).

This comes because - apart from log s in coupling constant - there are no dimensional parameters in QCD. Thus as σ has dimensions $1/p_\perp^2$, we get predictions. Experimentally the cross-section falls much faster than this - part of the effect can be understood from log Q^2/Λ^2 dependence. The rest is rather complicated but we believe we understand it. At much higher $p_\perp$'s (~ 50 GeV as in colliding beams) we do expect to find $1/p_\perp^4$ behavior.

In (ii) I commented that one needs to use independent production of resonances - not just individual particles - to describe low $p_\perp$ multiparticle production. It is attractive to consider that one is simply producing independent $q\bar{q}$ clusters which sometimes give single π's, sometimes pairs of π's, etc.

v) Scaling

To a reasonable approximation the invariant cross section is energy independent at large s, i.e., putting,

$$E\,\frac{d^3\sigma}{d^3p} = f(\sqrt{s}, p_\perp, x_{\parallel} = 2\,\frac{p_z}{\sqrt{s}}\ \text{c.m.}).$$

Then f scales, i.e., is energy independent for fixed $p_\perp$ and $x_\parallel$. This was first understood by Feynman. This energy dependence can be understood in Regge theory (using $\alpha_{\text{Pomeron}}(0) = 1$) using a formalism due to Mueller.

VI.H. Fermilab E350

I will now describe how one puts all the elements together in real experiments. I will naturally describe the apparati with which I have been associated - I know more about them.

I will describe first a very simple (by HEP standards) experiment - although as the thesis by Rosemary Kennett shows - a proper analysis of the data was a major effort. Perhaps because of the simplicity and elegance of the experiment and associated theory, the experiment was very succesful. The experiment was the 350th proposal at Fermilab - the third experiment at Fermilab with the photon detector which is the heart of the experiment. This detector was designed and built by Alvin Tollestrup (originally at Caltech, but now at Fermilab where he is playing a major role in the design and building of superconducting magnets) and Bob Walker.

The experiment is to study π^o's produced in $\pi^- p$ collisions. The simplest reaction is

$$\pi^- p \to \pi^o n \qquad (1)$$

or

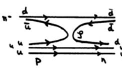

which was studied in one of the two earlier experiments at Fermilab.

E350 measured what is called an <u>inclusive</u> cross-section

$$\pi^- p \to \pi^o X \qquad (2)$$

where X includes all possible accompanying particles [i.e. $\pi^- p \to \pi^0 n + \pi^- p + \pi^0 \pi^- p + \ldots + \pi^- p \to \pi^0 \pi^+ \pi^- \pi^+ \pi^- \pi^0 \pi^0 n$ etc.]; given a π^0 specified by its kinematic parameters in the final state. Feynman introduced the term inclusive - in his terminology (1) is called <u>exclusive</u> because all particles besides those listed [the π^0 and n in (1)] are <u>excluded</u> from the final state. Feynman was the first physicist (I think) to point out that inclusive measurements were amenable to quantitative analysis.

Pictorally (2) can be pictured as

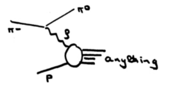

where the bottom part of the diagram is (virtual) ρ proton total cross-section. As we will study later, Mueller (a theoretician - now at Columbia) introduced the so-called triple Regge theory to describe the above picture quantitatively. We may remark here that in a simple quark picture the $\pi^- p$ total cross-section can be viewed as sum of cross-sections of q or $\bar{q}$ in π^- scattering off a proton target (the "additive quark model"). This picture is supported by approximate ratio

$$\frac{\sigma_{tot}(pp)}{\sigma_{tot}(\pi p)} = 3/2 \qquad (3)$$

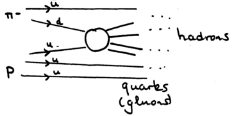

The above represents a typical $\pi^- p$ collision - note that the quark picture below (1) <u>is</u> a special case of this. Its justification must rest in (experiment) result than

$$\sigma_{tot}\ (q\ \text{on}\ q) \sim 1/6\ \sigma_{tot}(\pi^- p) \sim\ 4\ \text{mb} \tag{4}$$

For such a small qq, $\bar{q}q$ cross-section the chance of two or more quarks in say the proton both being involved in the collision is small. Using the formalism developed by myself and Wolfram ("Parton Showers" - CALT-68-755) it should be possible to make this intuitive picture more precise - this would be very important and I leave it to any reader wanting a quick Ph.D.

This physical picture also suggests that, as the heavier quarks (s,c...) are smaller than u, d (size ~ 1/mass) they will have smaller cross-sections. Thus

$$\sigma_{tot}(K^- p) < \sigma_{tot}(\pi^- p)\ \text{etc.} \tag{5}$$

This picture immediately suggests

$$\sigma_{tot}(\rho p) = \sigma_{tot}(\pi p) \tag{6}$$

as ρ and π have same quark structure. This prediction is consistent with experimental measurements - (2) is not terribly sensitive to (6) as (6) is for "real" π's and ρ's while (2) is only kinematically possible for off shell ρ's. The best tests of (6) come from photon processes where by vector dominance $\sigma_{tot}(\gamma p)$ can be related to the sum of $\sigma_{tot}(\rho,\omega,\phi,p)$, e.g. a sum of diagrams like

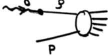

etc.

Such experiments (e.g. comparison of $\gamma p \to \rho p$ and $\gamma p \to \rho p$ which can be related to comparison of ρp and ϕp elastic scattering) confirm that the ϕ is indeed smaller than the ρ. One fly in the ointment is recent measurements of $\sigma_{tot}(\pi\pi \to \pi\pi)$ which come out smaller (by a factor of two) than the estimate (2/3 $\sigma_{tot}(\pi p)$) from the additive quark model. The experiment method used is indirect - it must use virtual π's (but as m_π^2 so small - these are very like real π's). Perhaps the analysis is incorrect - it is important to understand this.

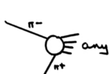

Process by which $\pi^-\pi^+$ total cross section is measured.

Before describing the experiment, let us describe the kinematics of the general inclusive reaction

$$ab \to cX \tag{7}$$

We can treat this as 2 → 2 scattering where the fact that we make no requirement on X means that we must add the mass m_X to the list of independent variables for 2 → 2 scattering. We remember that there were two independent variables usually taken as s and t. [$s = (p_a + p_b)^2$, $t = (p_a - p_c)^2$].

The triple (s,t,m_X^2) are a possible choice but instead of m_X^2 one usually uses the longitudinal momentum fraction

$$x_{\parallel}^{c.m.} = \frac{2\, p_z^{c.m.}|_c}{\sqrt{s}} \tag{8a}$$

where p_z is z component of momentum [initial particles a, b are along z direction] for the final particle c. In place of t one can also choose $k_\perp^2\big|_c$ - the square of transverse (i.e. $p_x\big|_c^2 + p_y\big|_c^2$) momentum of particle c. $k_\perp$ is naturally the same in both lab and c.m. system. There are in fact many different definitions of an "x" variable similar to (8a). Feynman first introduced x - which is often called "Feynman" x to distinguish it from "Bjorken" x which is used in electroproduction and neutrino scattering. Related variables to (8a) are

$$x_{\text{alternative}} = \frac{p_z^{c.m.}|_c}{p_z^{c.m.}|_{\text{maximum}}} \tag{8b}$$

$$\text{or} = 2\,\frac{|\vec{p}|^{c.m.}|_c}{\sqrt{s}} \tag{8c}$$

$$\text{or} = 2\,\frac{E^{lab}|_c}{E^{lab}|_a} \tag{8d}$$

The reader can show that (8b) - (8d) are essentially the same as (8a) in the limit

$x_{\parallel}^{c.m.}$ large ($\geqslant .3$)

$k_{\perp}^2$ small.

Note that $x_{\parallel}^{c.m.}$ has the kinematic range

$$-1 \le x_{\parallel}^{c.m.} \le 1 \tag{9}$$

The experiment was designed to study (2), $\pi^- p \to \pi^0 X$, in the kinematic region.

$$p_{lab} = 100 \text{ and } 200 \text{ GeV/c}, \ s \sim 2\, m p_{lab}$$

$$\sim 200 \text{ and } 400 \text{ GeV}^2.$$

$$x_{\parallel} \ge .7 \tag{10}$$

$$0 \le -t \le 4 \text{ GeV}^2 \quad . \tag{10}$$

[Remember that $t \le 0$ kinematically as discussed for $2 \to 2$ scattering.]

The apparatus is shown in figure VI.G.1 and we will now discuss the various parts of it.

(a) The detection of the final π^0 is done with a lead scintillator sandwich (shown in circular inset in VI.G.1) of a type described in VI.F. This sandwich measures the energy and position of the two photons produced in π^0 decay. The position is found by using a 70 x 70 hodoscope of scintillator (see VI.D.) As illustrated in VI.G.2, the matching ambifuities inherent in a hodoscope (i.e. the "ghost" photons mentioned in VI.D.) are not so severe as in a simple hodoscope because one measures not just "yes/no" but also the energy deposited.

(b) One trouble with inclusive reactions is that there are a multitude of other particles produced in the event to confuse the issue. The sweeping magnet in VI.G1 ensures that all (uninteresting) charged particles in the events miss the photon detector. As shown in VI.G.2, sometimes more than one π^o can sometimes hit the detector. Note that if n π^o's are produced in an event, these contribute n times to the inclusive cross-section (at the kinematic parameters of the individual π^o's). In particular

$$\int \frac{d\sigma}{dx_{\parallel}dt}(\pi^- p \to \pi^o n)\, dx_{\parallel}\, dt = \sigma_{total} \quad \langle n_{\pi^o}\rangle \tag{11}$$

where we integrate over the complete kinematic range of $x_{\parallel}$, t. $\langle n_{\pi^o}\rangle$ is the mean multiplicity of produced π^o's.

(c) We need to know the direction of the beam in order to calculate the $p_{\perp}$ (or t) of final π^o

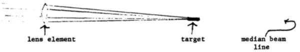

Notice that the beam particles are focussed at the target. One necessary reason for this is that the size of the target transverse to beam line is small compared to the size of transmitted beam. The focussing - depicted by a lens above - is performed by a pair of quadrupoles. A single quadrupole focusses in one view but defocusses in the other (these "views" are just two projections transverse to motion of beam). The theory of beams is quite fun; it is just like geometric optics (for thin beams) with magnetic dipoles to bend beam (equivalent to prisms) and quadrupoles to focus them (equivalent to lens). The size of a beam is determined by

(1) Initial angular acceptance and target size.

(2) Momentum spread within beam (a single dipole will obviously bend particles of different momenta by different amounts).

(3) Collimators and other physical obstructions restricting size of beam along its path.

(4) At low energy, multiple scattering is important (remember $\Delta p_\perp \sim$ const $\therefore$ $\Delta\theta_{\text{mult.scat.}} \sim 1/p$).

Let us describe the M2 beam line (See Art Ogawa, LBL-8305 Ph.D. thesis 1978 for further details and Fig. VI.G.3). This is one of the simplest beams possible; the beam used in the next experiment to be described involved 4 not 2 foci but the ideas are the same.

The quadrupole pair Q1, Q2 focusses the meson target at F1

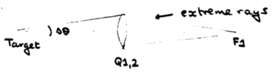

The angular acceptance ($\Delta\theta$) is determined by angle subtended by Q1,2 at target; naturally the larger this angle the larger is the number of particles one can transmit down the beam line. In between Q1,2 and F1 there is a bending magnet; the current in magnet determines the mean momentum transmitted; the geometry determines the momentum spread $\Delta p/p$. For this beam $\Delta p/p \approx 1\%$ (p range is $.99\ p_{\text{mean}}$ to $1.01\ p_{\text{mean}}$). For some experiments one needs a smaller $\Delta p/p$;

this can be achieved by closing the horozontal collimator C5. The beam is bent in the horizontal direction and as the target is very small (compared to the diameter 3" of beam pipe) the dispersion at F1 is solely due to momentum spread. Note that the beam is very small in vertical projection at F1 because this just reflects target size. Note the field lens at Q3 which focusses in the X (where beam is large due to momentum dispersion) and defocusses in the y view. One usually chooses vertical and horizontal foci to be in same position although this is not mathematically necessary. The path from F1 to F2 is essentially the inverse to that of target to F1. The bend B2 is arranged to exactly cancel momentum dispersion introduced by B1 so that whatever $\Delta p/p$, the image at F2 is small. Thereby we can use a target of reasonably small transverse directions! At 200 GeV momentum the size at F2 is 3 mm x 3 mm in transverse directions.

The theory of beams can be neatly set up in a matrix formalism. This is described in chapter 9 of Ritson's book and better in the "Transport" (a computer program used to design beams) manual. We at first denote a typical beam ray by a 2-dimensional vector (we have set up a co-ordinate system with z along the beam and x and y as the projections perpindicular to it)

$$\underline{V} = \begin{bmatrix} x \\ dx/dz \end{bmatrix} \tag{12}$$

Let $\underline{V}_{0,1}$ be value of this vector at $z = z_{0,1}$, then if $\underline{V}_{0,1}$ are connected by a field free region

$$\underline{V}_1 = M_D \, \underline{V}_0 \tag{13}$$

where M_D is a 2 x 2 matrix

$$M_D = \begin{bmatrix} 1 & \ell \\ 0 & 1 \end{bmatrix} \tag{14}$$

Now to discuss magnetic fields, we remember from Jackson that a charged particle travels in a circle of radius ρ in a uniform magnetic field B. In the diagram below, B is perpendicular to the paper.

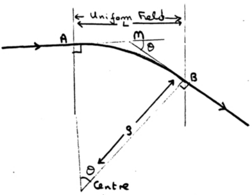

The radius of curvature ρ is given by

$$\rho = p/.03B \tag{15}$$

(ρ in meters, B in kilogauss, p in GeV).

Now as can easily be verified, for small angle deviations θ, one can approximate the circular path by a sharp bend of the same angle θ at the midpoint M of the uniform field region. Clearly for small θ

$$\rho\theta = L \tag{16}$$

and (15) becomes

$$p\theta = .03\ BL \tag{17}$$

Here $p\theta$ can be usefully viewed as a transverse momentum (perpendicular to original direction of motion) imparted by magnet to particle. (Remember total momentum of particle is unchanged by passing through field.)

A thin lens is a quadrupole field where

$$\left.\begin{array}{l} B_y = gx \\ B_x = gy \end{array}\right\} \quad \text{satisfies} \quad \nabla \times \underline{B} = 0 \tag{18}$$

Using (17) on x view, we see that it leads to a deflection that is proportional to distance from axis. For small L, (18) can be represented by 2 x 2 matrix

$$M_L = \begin{pmatrix} 1 & 0 \\ -1/f & 1 \end{pmatrix} \tag{19}$$

where $f = p/(.03\ gL)$.

i.e. lens leaves x unchanged but changes dx/dz by $-x/f$. Clearly f is focal length of lens. In the y view we find the same form for M_L with the opposite sign for f, i.e. this is a defocussing lens. It is clear that a single quadrupole will always focus in one projection and defocus in the other. However, a pair of quadrupoles of opposite sign separated by a drift space can be arranged to focus in both views. The reader can study this by looking at the product

$$\begin{pmatrix} 1 & 0 \\ -1/f_1 & 1 \end{pmatrix} \quad \begin{pmatrix} 1 & \ell \\ 0 & 1 \end{pmatrix} \quad \begin{pmatrix} 1 & 0 \\ 1/f_2 & 1 \end{pmatrix} \tag{20}$$

This illustrates the convenience of the matrix formulation: namely the total of successive elements is just gotten by calculating the 2 x 2 matrix product of the individual components.

When one considers a dipole or bend magnet one must extend formalism by using a 3 component matrix with $\Delta p/p$ added to x amd dx/dz in basic vector (12).

Note that the matrices (14) and (19) satisfy

$$\det M = 1 \tag{21}$$

This is no accident but rather Liouville's theorem that volume in phase space is preserved. e.g. suppose my beam is specified by the ellipsoid

$$\underline{V}^T E \underline{V} \le 1 \tag{22}$$

where if diagonal, E would have canonical form

$$E = \begin{pmatrix} 1/a^2 & 0 \\ 0 & 1/b^2 \end{pmatrix} \tag{23}$$

The area of phase space represented by (22) is proportional to $(1/\det E)^{1/2}$ (it is πab)

If $\underline{V}$ is transformed by M

$$\underline{W} = M \underline{V} \tag{24}$$

Then $\underline{W}$ satisfies

$$W^T M^{-1T} E M^{-1} \underline{W} \le 1 \tag{25}$$

and as long as det M = 1, the area of phase space is indeed preserved .

(d) An important aspect of nearly all high energy charged particle beams are Cherenkov counters. These enable one to tag the type (flavor) of the incident particle as π, K or proton. At low energies one uses the fact that for fixed momentum the effect of an electrostatic field is $\propto 1/\beta = c/v$ and so bends particles of different flavors by different amounts. Thereby one can prepare a beam containing one flavor; this is called a separated beam. It is most useful for the "uncommon" particles like $K^{\pm}$ or $\bar{p}$ which are small percentage (1/2 to 5%) of a beam. Unfortunately, at high energy β is so near 1 that this method does not work. So one must be content with tagging on an event by event basis the flavor of a particle. One might think that this was as good but it often is not. Thus a typical apparatus can only take a certain maximum intensity ($10^6 \to 10^7$ particles/second for large aperture systems). Note this is determined not by events of interest (for which one designs a trigger to reduce sample to write on tape of $10 \to 100$ events/second) but by uninteresting events - the particles of which produce signals in our detectors whose effect must be cleared out before we can record an event of interest. Thus it is harder to study $K^{\pm}$, $\bar{p}$ with precision at Fermilab because one's effective maximum incident flux is reduced by the beam fraction ratio of $1/2 \to 5\%$.

The general theory of a Cherenkov counter is described on pages 638-641 of Jackson's electricity and magnetism book but one does not need to understand this detailed theory to be able to understand its use in high energy physics (a summary for this purpose may be found in senior thesis Bill Danchi wrote for me two years ago).

A particle traveling through a medium of refractive index n emits light at angle θ determined by

$$\cos\theta = 1/\beta n \,. \tag{26}$$

The requirement $\cos\theta \leq 1$ (!) implies

$$\beta > 1/n \tag{27}$$

In our case, $\beta = p/E = p/\sqrt{m^2 + p^2} = (1 + m^2/p^2)^{-1/2}$ and for $p \gg m$, this becomes

$$= 1 - m^2/2p^2.$$

If $n = 1 + \delta n$ is very near 1, (27) becomes the condition

$$m^2/2p^2 > \delta n$$

or

$$p > \frac{m}{\sqrt{2\delta n}} \tag{28}$$

Thus light is emitted if the particle momentum is greater than some threshold value p_{th} that is linearly porportional to m. In our beam, we have a fixed momentum p. We tell the particle types π, K or p from their different masses. For instance, suppose we use a C counter with δn such that

$$p_{th}(K) > p > p_{th}(\pi)$$

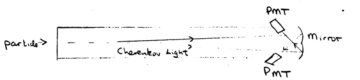

(PMT=phototube)

The light is emitted in the above counter if the beam particle is a π but not if it is a K or a p. The refractive indices near 1 (δn << 1) are obtained by filling counter with helium and reducing pressure appropriately. One could tell in principle all 3 beam types with a second counter whose threshold is set between that for K's and protons.

Then a π gives a signal in counter #1 and #2; a K gives a signal in counter #2 only; a p gives a signal in neither counter.

At high energy this is not adequate as even for long counters only a few photons are emitted. Thus counter #1 will fail to fire on π's quite often (a typical inefficiency is $5 \rightarrow 20\%$ at 200 GeV). Thereby a π would look like a K 5 to 20% of the time; unfortunately as we said there are typically < 5% kaons in the beam and so the "K sample" defined by the above criterion would in fact have more π's than K's in it! One can remedy this either by using several counters ($(5\%)^2$ is quite small) or by using the additional information contained in angle of Cerenkov radiation. The type of counter described above is called a "threshold counter." The new type of Cherenkov counter is called a "DISK" counter. A typical geometry is shown below (there are many variations on this).

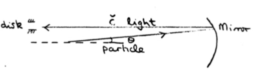

The annular disk (for normal cylindrical geometry) selects light emitted a particular angle θ. (26) gives the dependence of θ on β and hence particle type. Unlike the previous (crude) threshold counter, the disk counter depends on the initial particle beam being (approximately) parallel. This is easy enough to arrange using suitable beam elements, e.g. in VI.G.3 we could put Q4, 5 so that F1 was at their focus and a parallel beam would then pass through the downstream C counter. One would of course need an extra quadrupole doublet to focus this parallel beam onto the target.

A typical use of a disk counter would be to run above K threshold so that K's and π's give light. Then one chooses the disk size to select K but not π

light. This gives a positive K signature which is unaffected by π inefficiency.
(e) We finally return to the experiment. The beam direction on an event by event basis is measured by the four sets of scintillation counter (two in each view) marked UX, UY, DX, DY in Fig. VI.G.1. Each set has six fingers looked at by an individual photon multiplier tube (PMT). One uses them as a straightforward hodoscope system described in VI.D (p. 9). As there is only one particle in beam one has no difficulty with ghost particles. The downstream counters are very small ($1/16^{th}$ inch) and so one gets the intercept at target with an accuracy (standard deviation) of $1/(16 \times 2\sqrt{3})$ inch.

Essentially the only other part of the apparatus are further scintillation counters. M1, 2, 3 make certain that the beam is indeed heading towards the target and that there is only 1 particle in beam. The counters A0, 1, 2, 3 4 are used as yes/no devices to signify events with <u>no</u> charged particles at all in final state. Examples are

$$\pi^- p \rightarrow \pi^o n$$

$$\pi^- p \rightarrow \pi^o \pi^o n \quad \text{etc.}$$

As described in Rosemary Kennett's thesis there is a rather pretty theory to apply to such final states. As we only use A0 - 4 to tell 0 from >0 particles, we have no problems with Landau tails and we can see a clean signal of the all neutral final state. (There is some problem with δ rays produced by π^- beam traversing target and striking A0 - 4. These make a true all neutral final state look like one with charged particles in it.)

In each view
70 Scintillation counters
1 cm wide 0.7 cm thick
Each counter is 8 rods joined to Same PMT

E350 Apparatus

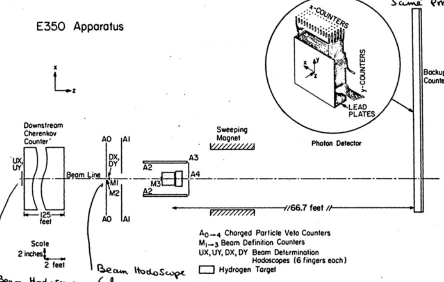

Beam Hodoscope
6 fingers
each finger
9.25 mm
wide

Beam Hodoscope
6 fingers
each finger
1.57 mm wide

Fig. VI G.1

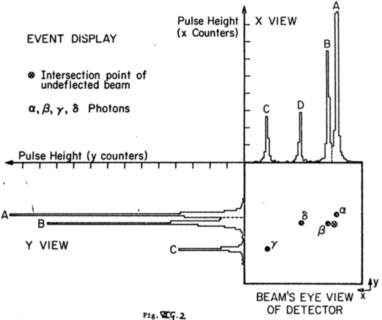
EVENT DISPLAY
⊗ Intersection point of undeflected beam
α, β, γ, δ Photons
Pulse Height (x Counters)
X VIEW
A
B
C
D
Pulse Height (y counters)
A
B
Y VIEW
C
δ
α
β
γ
y
x
BEAM'S EYE VIEW OF DETECTOR

Fig. VI.2

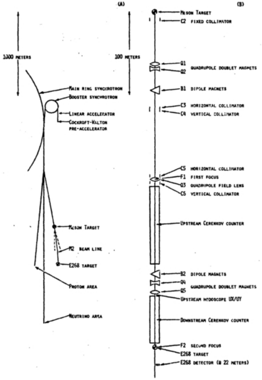

XBL 7810-11703

Fig. S1-1 (A) Fermilab proton synchrotron and experimental areas. (B) M2 beam line optics (schematic).

fig VI.3

VI.I. Fermilab E110 and E260

VI.I.1 The Experiment

The new feature of this experiment shown in Fig. VI.H.1 is the detection of charged particles in the final state. It is not practical to use scintillation hodoscopes to detect particles over large angular regions and so we cannot use same method described for beam particle in E350. We detect charged particles by ionization not in scintillation counters but in wire chambers. For information on chambers, see the article by Charpak in Physics Today (Oct., 1978) and book by Rice-Evans (Spark, Streamer, Proportional and Drift Chambers) in the Lauritsen Downs Library.

As in the beam discussion of VI.G, we set up axes with x horizontal, y vertical and z along the initial beam direction. We measure direction and total momentum of charged particles in the final state. The direction comes from observing intersection in at least 2 wire chambers. The momentum comes from bend in a magnetic field. For the vertical field used in the experiment, the charges $\delta\theta_x$, $\delta\theta_y$ produced by magnet are,

$$\delta\theta_y = 0 \tag{1}$$

$$\delta\theta_x = \frac{.03 \int B\, d\ell}{p_z} \tag{2}$$

Typical values would be $B \sim 20$ kg (2 tesla), $\ell = 1 \rightarrow 3$ meters so that (2) is about

$$\delta\theta_x \sim 1/p_z \quad \text{radians} \tag{3}$$

Note this is a small change in angle for high energy particles with p_z taking values up to 200 GeV in our experiment. So one needs to measure directions well. One has chambers separated by $1 \rightarrow 5$ meters and measures intersection to

PLAN VIEW MULTIPARTICLE SPECTROMETER DEC 1975 – JAN 1976 BERYLLIUM TARGET RUN

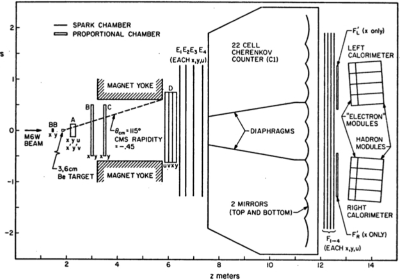

fig VIII.1

a fraction of a 1 mm. Thus an error in $\delta\theta$ of 10^{-4} is not hard to obtain*. (3) then implies that

$$\delta p_z/p_z^2 \sim 10^{-4} \tag{4}$$

This implies that fractional error in momentum measurement $\delta p_z/p_z$ is approximately 10^{-4} p_z, i.e., linear in p_z. At 200 GeV we get a 2% measurement for our nominal 10^{-4} error. There are other contributions to δp_z; in particular multiple scattering discussed in VI.E. is important at low energy.

There are 3 basic types of wire chambers:

spark chambers

proportional chambers (PWC)

drift chambers.

I will not discuss spark chambers. They are essentially obsolete. They are cheaper than proportional or drift chambers. Their main disadvantage is that (i) they are "dead" for $\sim$ 10 milliseconds after recording an interaction; (ii) they cannot resolve close together tracks (although their resolution on a single track is as good as a PWC.)

VI.I.2 Proportional Chambers (PWC)

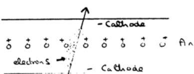

We show above a view looking straight down on chamber. Thin parallel wires

*For configuration on handout, $\delta p_z/p_z^2 \sim 7 \times 10^{-4}$. This is dominated by short lever arm (separation $\sim$ 1 meter, $\sigma^2 \sim 1/2$ mm) in front of magnet.

form the anodes and the walls of the chamber the cathode. The chamber is filled with gas. The electrons drift to the nearest anode for low fields, there is a pulse on each wire approximately equal to the ionization produced by incident particle. As the field increases the drifting electrons are accelerated and when they reach high enough energy, secondary ionization is produced. This can amplify pulse on wire by a large factor ($\sim 10^5$) allowing its detection with simple electronics. Note that the field ($\propto 1/r$, r distance from an anode center) is large near anodes and the avalanche of secondary ionization is located very near wire. The chambers are called "proportional" because size of pulse on anode is still approximately proportional to initial ionization. When field gets too big the output pulse saturates at a value independent of input ionization; this is regime used in a geiger counter.

The main expense in a PWC is the electronics which cost about $10 per wire. Systems with up to 10^5 wires are not uncommon. The wire spacing can be as small as 1/2 mm but 2 mm gives a resolution $\sigma = 2/2\sqrt{3} \sim 0.6$ mm. As mentioned one uses measurements from several chambers to reduce this error.

VI.I.3 Drift Chambers

This type of chamber is similar to a PWC except that one arranges wires much further apart and has an electric field

wires

$0 \longleftrightarrow 0$

~ 5 cm

That is essentially constant except in immediate vicinity of anode wire. This is done by suitable placing of cathode and field shaping wires. The time of arrival of an electron at anode is then directly proportional to the distance from it that electron (ionization) was produced. So with the sophisticated electronics one records not only existence of a pulse but also its time to arrival. As the drift time is 0(20) nanoseconds per mm, a time resolution of 2 nanoseconds gives an accuracy of .1 mm. This is better than a PWC.

Drift chambers are cheaper than PWCs for large drift spaces and large chambers. They have the disadvantage of a comparitively long dead time because one has to allow 200 nanoseconds/cm for electrons to drift. A normal PWC with 2 mm wire spacing can recover in about 50 nanoseconds. However drift chambers are superior to spark chambers for dead time.

VI.I.4 Rest of E260

There are other components in Fig. VI.H.1. In particular:

(1) Cherenkov counters to tell type (π, K, p) of final charged particles (not just of beam particle as in VI.G.). These are of "threshold" type. One cannot easily use a disc counter because the light rays produced by $\check{C}$ radiation are not parallel or even diverging from a point (due to magnet bend); thus there is no simple optics to select a particular $\check{C}$ angle of emission. "Disk" like counters are being designed that would work in situations like this. They essentially detect (x,y) co-ordinates of all light incident on an area and so see the "circle" associated with the particle. I don't think any devices of this type work yet.

(2) Calorimeters. We have already discussed these in VI.B. and VI.F.

i.e.,

$$P|q:\underline{p},\lambda_W\rangle = +|q:-\underline{p},+\lambda_W\rangle$$
$$P|\bar{q}:\underline{p},\lambda_W\rangle = -|\bar{q}:-\underline{p},+\lambda_W\rangle \tag{9}$$

for quarks and antiquarks. For bosons, parity of particle and antiparticle is equal. Also the parity of particles in the same multiplet is equal, e.g., p and n have the same parity as do $\pi^{\pm}$ and π^{o}.

Also note that <u>some</u> parity assignments are arbitrary. For instance, there is always an even number of fermions in a reaction. Thus if I multiply the parity of all fermions by -1, it cannot affect anything (as all that appears is product of parities and so this product always contains an even number of fermions, i.e., $(-1)^{\text{even number}}$). Such arbitrariness is present with other quantum numbers. It is called a superselection rule.

<u>Examples</u>

(A) <u>$\eta \to \pi^{o}\pi^{o}$ (or $\pi^{+}\pi^{-}$)</u>

Each particle in the candidate decay has $\eta_p = -1$ and spin 0. Thus (7) gives $M_{ooo} = -M_{ooo}$, i.e., reaction is forbidden.

To apply (8), we find $\ell_{ab} = 0$ by spin addition and thus (8) reads $-1 = (-1).(-1).(+1)$ again forbidding reaction.

(B) <u>$\rho^{o} \to \pi^{+}\pi^{-}$</u>

Again all $\eta_p = -1$ but now ρ has spin 1. In (7), all λ are still zero but $(-1)^{s_A}$ saves the day and $M_{ooo} = +M_{ooo}$.

The reaction is allowed in accord with experiment. In the orbital angular momentum formalism $\ell_{ab} = +1$ and (8) is satisfied.

(C) $\underline{A^-_{1,2} \to \pi^- \eta}$

Here $J_a = J_b = 0 \qquad \eta_{P_a} = \eta_{P_b} = -1.$

$J_A = 1 \qquad \eta_{P_A} = +1.:A_1$

$J_A = 2 \qquad \eta_{P_A} = +1:A_2$

The A_1 decay is forbidden and the A_2 allowed.

(D) Determination of Parity of the Pion (p.83 Perkins)

In analyzing the constraints on the two body process $ab \to cd$, we essentially insert a complete set of states of arbitrary total spin J_A and parity η_{P_A}.

$$\begin{aligned} T(ab \to cd) &= \sum_{J_A, \eta_{P_A}} T(ab \to A) T(A \to cd) \\ &= \sum_{J_A, \eta_{P_A}} T(A \to ab) T(A \to cd). \end{aligned} \tag{10}$$

We will later see how to do this in detail for the helicity formalism. Now we consider a particular example $\pi^- d \to nn$ in the orbital angular momentum analysis. Here we choose angular momenta ℓ_{ab}, ℓ_{cd} and total spin J_{ab}, J_{cd} independently for initial and final states. J_{ab} and ℓ_{ab}; J_{cd} and ℓ_{cd} are combined to give the same total spin J_A and the same parity η_{P_A}. Parity conservation will imply the constraint

$$\eta_{P_a} \eta_{P_b} (-1)^{\ell_{ab}} = \eta_{P_A} = \eta_{P_c} \eta_{P_d} (-1)^{\ell_{cd}}. \tag{11}$$

We observe $\pi^- d \to nn$ at low energies. One advantage of the angular momentum formalism is that typically an amplitude of orbital angular momentum ℓ behaves like $p_{ab}^{\ell_{ab}}$, $p_{cd}^{\ell_{cd}}$. Here p_{ab}, p_{cd} is (center of mass) momentum derived in IV.B. Thus low energy processes are dominantly s waves ($\ell = 0$). There is no simple way to express this constraint in terms of helicity amplitudes.

We first analyze the $\pi^- d$ system. The deuterium is a bound state of p and n in s (and) d wave. It is spin-parity 1^+. Pion has parity η_π (which we want to find). Analysis of $\pi^- d$ system therefore implies $J_A = 1$ and $\eta_{p_A} = \eta_\pi$.

We now consider the nn system. Combining $J_c = J_d = 1/2$, we get $J_{cd} = 0$ or 1. For each J_{cd} state we can choose $\ell_{cd} = 0,1...$ Note that we can have $\ell_{cd} > 0$ because at threshold $p_{ab} = p_{\pi^- d} = 0$, we have $p_{cd} > 0$ as $m_{\pi^-} + m_d > 2\, m_n$.

We constrain ℓ_{cd} by (Pauli) principle that any state of identical fermions must be odd under the interchange of the fermions. Looking at the explicit values of the Clebsch-Gordon coefficients, we see that the $J_{cd} = 1$ state is symmetric and $J_{cd} = 0$ antisymmetric under the interchange $c \leftrightarrow d$. The general symmetry result comes from the relation

$$C(s_1 m_1 s_2 m_2 | sm) = (-1)^{s-s_1-s_2} C(s_1 {-m_1}\; s_2 {-m_2} | s{-m}). \tag{12}$$

In our case, $s_1 (\equiv J_c) = s_2 (\equiv J_d) = 1/2$ and so $J_{cd} = s = 1$ gives +1 and $J_{cd} = s = 0$ the phase -1 under interchange.

Thus we need $\ell_{cd} = 0,2$ ... for $J_{cd} = 0$

$\ell_{cd} = 1,3$ ... for $J_{cd} = 1$.

We can only get total spin $J_A = 1$ from combining $\ell_{cd} = 1$ with $J_{cd} = 1$. The parity η_{p_A} is then $(-1)^{\ell_{cd}} = -1 = \eta_\pi$. We thus find that the π has negative intrinsic parity. Notice Perkins says that the above argument depends on the assumption that n and p have the same parity. I believe this is a necessary fact; there is no superselection rule allowing one to assign different parities to n,p. As they are related by simple internal symmetries, they must have the same parity.

(E) Positronium

This is a bound state of e^+ and e^- analogous to the hydrogen atom. As in nn example, the total spin $J_{ab} = 0$ or 1, while $\ell = 0, 1, 2 \ldots$ for each J_{ab} choice.

Now act with C; we get back the same state with e^+ and e^- interchanged and no phases ($\eta_i\eta_{\bar{I}} = 1$ for C). But the symmetry on interchanging particles is $(-1)^{\ell}$ times (-1) $J = 0$ and $(+1)$ $J = +1$; this can be written $(-1)^{\ell + J_{ab} + 1}$. However, we pick up another extra minus sign because we must also interchange two operators defining states. Thus if $a^{\dagger}$ $(e^{\pm})$ is operator creating an $e^{\pm}$, then our initial e^+e^- state is $a^{\dagger}(e^+)a^{\dagger}(e^-)|0\rangle$ where $|0\rangle$ is vacuum state. Then acting with C gives $a^{\dagger}(e^-)a^{\dagger}(e^+)|0\rangle = -a^{\dagger}(e^+)a^{\dagger}(e^-)|0\rangle$ as any two fermion operators must anticommute. Therefore, C acting on state gives $-(-1)^{\ell + J_{ab} + 1} = (-1)^{\ell + J_{ab}}$. Note Perkins has a funny argument for this extra - sign which is dubious to say the least.

If we consider the n photon decay of positronium, $e^+e^- \to n\gamma$. Then $(-1)^n = (-1)^{\ell + J_{ab}}$ as C acting on final state is $(-1)^n$.

For the ground state, $\ell = 0$ and so we see that $J_A = J_{ab} = 0$ state (parapositronium) decays into 2 photons while the state $J_A = J_{ab} = 1$ (orthopositronium) decays into 3 photons.

IV.F 2 Particle → 2 Particle Scattering

IV.F.1 Spinless Particles: The Mandelstam Variables

Consider the general reaction

$$ab \to cd \tag{1}$$

where particle i has mass m_i. The transition amplitude is $M = \langle cd|T|ab\rangle$, the matrix element of the Lorentz invariant operator T. If we have spinless particles, then M is a function of the possible Lorentz invariants one can form from the momenta p_i. Apart from the masses $p_i^2 = m_i^2$, these are

$$\begin{aligned} s &= (p_a+p_b)^2 = (p_c+p_d)^2 \\ t &= (p_a-p_c)^2 = (p_b-p_d)^2 \\ u &= (p_a-p_d)^2 = (p_b-p_c)^2 \end{aligned} \tag{2}$$

where, of course,

$$p_a + p_b = p_c + p_d \tag{3}$$

expresses energy momentum conservation for the process. One can easily prove from (2) and (3) that

$$s + t + u = \sum_{i=1}^{4} m_i^2 \tag{4}$$

and so for fixed external particles and hence fixed masses, there are two independent invariants which we can take to be s and t. s, t and u are often called the Mandelstam variables.

To understand the interpretation of the variables, let us consider a typical experimental set up. Namely, a beam of particles a of some fixed momentum p_{lab} is incident on a target of particles b which is at rest. b is usually a proton but can also be a deuteron, heavier nucleus or even an electron. There is a wide variety of choices for a = π, K, p, e, μ, γ, ν, etc.

Let a travel in the positive z direction so that the four vectors of a and b are

$$
\begin{aligned}
p_a &= (0,0,p_{lab},\sqrt{m_a^2+p_{lab}}) \\
p_b &= (0,0,0,m_b).
\end{aligned}
\tag{5}
$$

Then $s = (p_a+p_b)^2 = p_a^2 + p_b^2 + \underbrace{2p_a \cdot p_b}_{\text{4 vector product}} = m_a^2 + m_b^2 + 2m_b\sqrt{m_a^2 + p_{lab}^2}$. Generally

$p_{lab} >> m_a, m_b$

$$
\begin{aligned}
\therefore s &\approx 2m_b p_{lab} \\
&\approx 2p_{lab} \text{ for proton targets.}
\end{aligned}
\tag{6}
$$

The latter approximation is worth remembering. Note that in p nucleus collisions, the effective s is still given by (6) with $m_b \sim$ proton mass, as except for coherent reactions (which are normally independent of s anyway) the incident proton collides not with the whole nucleus but with the individual protons (or even more precisely quarks) inside the target.

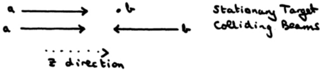

Another interesting case is that of colliding beams where normally a = b or antiparticle $\bar{b}$ (for pp, $\bar{p}$p and e^+e^- machines). The kinematics is particularly transparent when a and b have equal but opposite momenta. [True when a and $\bar{b}$ are accelerated in the same ring as for e^+e^- and $\bar{p}$p collisions. In pp colliders one needs two rings and at Fermilab the rings will be run at different momenta.] The four vectors are now

$$p_a = (0,0,p_{lab},\sqrt{m_a^2+p_{lab}^2})$$
$$p_b = (0,0,-p_{lab},\sqrt{m_a^2+p_{lab}^2}) \tag{7}$$

and

$$s = 4(m_a^2+p_{lab}^2)$$
$$\sim 4p_{lab}^2. \tag{8}$$

For a given size ring, i.e., a given maximum momentum p_{lab}

$$\frac{s(\text{colliding beam})}{s(\text{stationary target})} \sim 2p_{lab}. \tag{9}$$

As the cost of stationary target machine is proportional to p_{lab}, it follows that it is much more efficient to build colliding beams to get to high energy than to build a bigger stationary target machine. All the new machines planned involve colliding beams. Notice there is one problem with the latter that interaction rate is much lower as beam is much lower density than a target of liquid hydrogen.

In summary, we can regard s as specifying the initial energy of reaction. Now we will interpret t (or u) which we see can be viewed as specifying the scattering angle.

First note that in a typical reaction $e^-p \to e^-p$

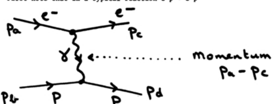

$t = (p_a - p_c)^2$ is the square of four vector carried by virtual photon. When we discuss the Feynman rules quantitatively, we will learn that in a diagram (the lowest order "Born term"),

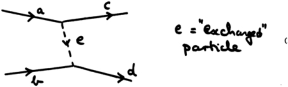

(10)

the amplitude is proportional to $1/(t-m_e^2)$ where m_e is the physical (on shell) mass of the virtual particle e. Thus t certainly has an important dynamical significance; in (10) e corresponds to the force "causing" scattering and approximately the Yukawa potential

$$1/r \exp[-m_e r]. \tag{11}$$

As very different examples contrast

A. $e^- p \to e^- p$, where virtual photon with $m_e = 0$ is exchanged.
$\uparrow\uparrow \quad \uparrow\uparrow$
$a\ b \to c\ d$

The amplitude is proportional to $1/t$ or from (11) the potential is $1/r$ (i.e., long-range and not exponentially damped as for $m_e > 0$).

B. $\nu_\mu n \to \mu^- p$

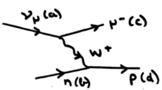

(12)

Here, on the other hand, the amplitude is proportional to $1/[t-m_W^2]$. This is a short range $[r \sim 1/m_W$ from (11)] force and for low energies [we will learn soon that kinematic range of t is approximately $0 \geq t \geq -s$], the propagator $1/[t-m_W^2]$ can be approximated by $1/m_W^2$. In fact, we have already used one consequence of this, i.e., in a unified theory, the vertices in (12) are just α e, and so strength of weak interactions is $e^2/m_W^2 \sim G_F$, to estimate m_W from observed value of Fermi constant G_F.

Now let us try to interpret u. Consider $dG \to dG$. This has three low order QCD diagrams.

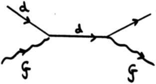

$\propto 1/(s-m_d^2)$ (13a)

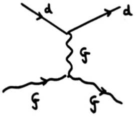

$\propto 1/t$ (as gluon mass exactly zero) (13b)

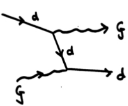

$\propto 1/(u-m_d^2)$ (13c)

and the third diagram illustrates that u as well as t can have dynamical significance. Notice that u and t can be interchanged by simply relabeling the final particles, i.e., $u \leftrightarrow t$ if we put c = G, d = d quark instead of c = d quark, d = G as used in (13). One tends to write reactions (as $dG \to dG$ not

$dG \to Gd$ for example) in such a way that t appears more often than u in the dynamical equations. We refer to the three diagrams (13a,b,c) as s, t and u channel diagrams (or "exchange" diagrams), respectively. Again note that $e^-p \to e^-p$ has only t channel and no s or u channel diagrams; $e^+e^- \to q\bar{q}$ has s and no u or t channel diagrams; $e^+e^- \to e^+e^-$ has s and t but no u channel diagrams.

We now consider the kinematic interpretation of t and u. [We have learned that s is the square of total energy in c.m.s..] Consider the reaction (1) in the overall c.m.s. of ab or cd. Choose the axes so that a is along positive z axis, b along negative z axis and c,d in xz plane. Let the 3 vector of c make angle θ with that of a in this frame.

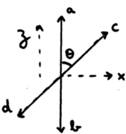

Then we can easily find the explicit forms of the four vectors as follows (cf. II.B)

$$p_a = (0,0,p_{ab},E_a)$$

$$p_b = (0,0,-p_{ab},E_b)$$

$$p_c = (p_{cd}\sin\theta,0,p_{cd}\cos\theta,E_c) \tag{14}$$

$$p_d = (-p_{cd}\sin\theta,0,-p_{cd}\cos\theta,E_d)$$

where

$$E_a = \frac{s + m_a^2 - m_b^2}{2\sqrt{s}} \qquad E_b = \frac{s + m_b^2 - m_a^2}{2\sqrt{s}}$$

$$E_c = \frac{s + m_c^2 - m_d^2}{2\sqrt{s}} \qquad E_d = \frac{s + m_d^2 - m_c^2}{2\sqrt{s}} \tag{15}$$

and

$$p_{ab} = \lambda^{1/2}(s,m_a^2,m_b^2)/2\sqrt{s}$$

$$p_{cd} = \lambda^{1/2}(s,m_c^2,m_d^2)/2\sqrt{s}. \tag{16}$$

Now we can calculate

$$\begin{aligned} t &= (p_a-p_c)^2 \\ &= m_a^2 + m_c^2 - 2p_a\cdot p_c \\ &= m_a^2 + m_c^2 - 2E_aE_c + 2p_{ab}p_{cd}\cos\theta \end{aligned}$$

or

$$\begin{aligned} \lambda^{1/2}(s,m_a^2,m_b^2)\lambda^{1/2}(s,m_c^2,m_d^2)\cos\theta &= s(t-u) + (m_a^2-m_b^2)(m_c^2-m_d^2) \\ &= 2st - s(\Sigma_i m_i^2)+s^2+(m_a^2-m_b^2)(m_c^2-m_d^2). \end{aligned} \tag{17}$$

We see that for fixed s, $\cos\theta$ is linearly related to t and so:

> choice of variables s and t is equivalent to <u>incident energy</u> and <u>scattering angle</u>. t is natural for scattering angle between a and c; u between a and d.

Naturally on interchanging $t \leftrightarrow u$ [and $m_c \leftrightarrow m_d$], one finds from (17) that $\cos\theta \to -\cos\theta = \cos(\theta+\pi)$ where $\theta + \pi$ is the angle between a and d.

Let us investigate the kinematics in the very simple case $m_i^2 = 0$ which always gives the leading order results at high energies. Then (17) becomes $\cos\theta = (t-u)/s$ or using (4), $\cos\theta = 1 + 2t/s = -1 - 2u/s$.

As the physical region is $-1 \le \cos\theta \le 1$, we see that t,u lie in range

$$0 \ge t,u \ge -s. \tag{18}$$

This can be usefully illustrated in a two dimensional plot of s v. t.

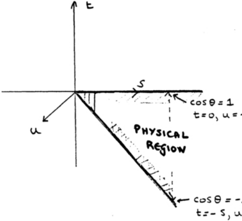

dominated by s-channel diagrams

t-channel

u-channel

The physical region is contained between the solid black lines which are $t = 0$ and $u = 0$. Notice that constant u contours are straight lines at $-45°$ to the s axis [as $s + t + u = 0$]. More elegantly but not particularly usefully, one can use s, t, u axes that are symmetrically placed at 60° to each other. The kinematic diagram makes it clear that regions of small t and small u are kinematically distinct at high energies

small t enhances $\frac{1}{t - m^2}$, i.e., t-channel diagram

small u enhances $\frac{1}{u - m^2}$, i.e., u-channel diagram

so t,u channel diagrams dominate in very different kinematic règimes.

We will return to this picture when we discuss the analytic structure of the scattering amplitude.

IV.F.2 Partial Wave Expansion for Spinless Particles

Let us try to relate the above to our orbital angular momentum formalism. If the particles are spinless, the initial and final orbital angular momenta ℓ_i and ℓ_f are equal to each other and to the total spin J of the system. One can describe a reaction either by its s and t dependence or by its s and J dependence. J is conjugate directly to the variable $\cos\theta$; as t is linearly related to $\cos\theta$, J is essentially a conjugate variable to t. The relation between J and $\cos\theta$ is simply

$$M(s,t) = \sum_J (2J+1) M_J(s) P_J(\cos\theta) \tag{19}$$

or

$$M_J(s) = \frac{1}{2} \int_{-1}^{+1} M(s,t) P_J(\cos\theta) d(\cos\theta). \tag{20}$$

When is J,s a convenient description and when is s,t convenient?

A. If there is a dominant s channel diagram (or a few of them) then J will have a definite value, e.g.,

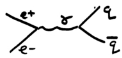

and clearly $M_J(s)$ is much the best parameterization. This is also true at low energies in hadron hadron scattering

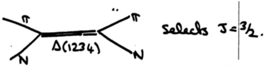

B. At high energies in hadron hadron scattering, a huge number of J values are present and the s,J description becomes very clumsy. A classical argument suggests the number of J values.

$$J \sim \text{momentum x distance} \tag{21}$$

where momentum $\sim p_{ab}, p_{cd} \sim \sqrt{s}/2$ at high energies. The "distance" in (21) is the impact parameter b. To find this, consider nucleons as spheres of radius 1 Fermi. Then the diagram below shows the maximum b for which there is still scattering.

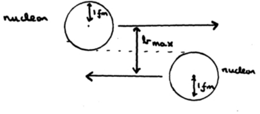

Thus $0 \le b \le b_{max} \sim 2$ fm ~ 10 GeV^{-1} or

$$0 \le J \le 5\sqrt{s} \tag{22}$$

where $\sqrt{s}$ is measured in GeV. At Fermilab energies $p_{lab} \sim 400$ GeV, we find $J \le 150$, i.e., as claimed, a plethora of partial waves contribute.

Actually there is no "sharp" cutoff but the scattering cross-section falls exponentially (remember $V \sim 1/r \exp(-mr)$ with $r \sim b$) above the limit (22).

IV.F.3 Partial Wave Expansion for Particles with Spin

When considering particles with spin, we have learned qualitatively how to use the orbital angular momentum formalism in the discussion of $\pi^- d \to nn$ in IV.E. However, this is usually rather a clumsy way of expressing angular ($\cos\theta$) variation of a scattering amplitude for particles with spin (compare IV.D (3) and (17)).

Consider the reaction (1) for particles with spin J_i (i = a, b, c, d). Then the scattering amplitude $\langle cd|M|ab\rangle$ is a matrix element of M between (two) particle states whose momenta are given in IV.F (14). Let us suppose spin content of states is specified in the helicity formalism, i.e., each particle has helicity λ_i with $-J_i \le \lambda_i \le J_i$. Then the reaction is described by "helicity amplitudes" $M_{\lambda_a\lambda_b\lambda_c\lambda_d}$

$$M_{\lambda_a\lambda_b\lambda_c\lambda_d} = \langle c[p_c,\lambda_c]\ d[p_d,\lambda_d]|M|a[p_a,\lambda_a]\ b[p_b,\lambda_d]\rangle. \qquad (23)$$

For each choice of indices λ_i, M is a function of s, t and u which enjoy the same kinematics and interpretation given in IV.F.2. The introduction of J given in IV.F.2 for the spinless case (where J = orbital angular momentum) can formally be regarded as the "Clebsh-Gordon" problem for the Poincare group, i.e., the direct product of representation a by representation b is decomposed into irreducible representations of the Poincare group. This is most convenient in the a,b c.m.s. as the product representation has momentum vector $p_a + p_b$ and c.m.s. corresponds to our "standard" choice of p_R for a system with $p_R^2 = (p_a+p_b)^2 > 0$. The Lorentz invariance of M implies that a,b and c,d combine to give systems of same total spin J (and parity). Formally we can proceed by introducing a complete set of states.

$$\begin{aligned} M &= \langle cd|M|ab\rangle \\ &= \sum_{\substack{J_i\mu_i \\ J_f\mu_f}} \langle cd|J_f\mu_f\rangle\langle\mu_f J_f:\lambda_c,\lambda_d|M|\mu_i J_i:\lambda_a,\lambda_b\rangle\langle J_i\mu_i|ab\rangle \end{aligned} \qquad (24)$$

where i,f denote initial, final, respectively. μ_i, μ_f are spin components along z direction for states (which are at rest because we work in ab,cd c.m.s.) of spin J_i and J_f, respectively. In (24), $\langle J_f\mu_f|M|J_i\mu_i\rangle$ must also have labels λ_i because the labels J_i and μ_i do not define state, i.e., states of these quantum numbers can be gotten with several different choices of λ_a, λ_b [(26) is only the constraint]. The Lorentz invariance of M implies that

$$<\mu_f J_f : \lambda_c, \lambda_d | M | \mu_i J_i : \lambda_a, \lambda_b> \propto \delta_{\mu_i \mu_f} \delta_{J_i J_f}. \tag{25}$$

Now for the choice IV.F (14) with a,b along z axis, we have from IV.D (1)

$$\mu_i = \lambda_a - \lambda_b \tag{26}$$

while IV.D (3) and (6) imply that $<cd|J_f \mu_f>$ is proportional to

$$d_{\mu_f, \lambda_c - \lambda_d}(\theta). \tag{27}$$

Combining (24) to (27), we find the analog of (19) for particles with spin - namely,

$$M_{\lambda_a \lambda_b \lambda_c \lambda_d}(s,t,u) = \sum_J (2J+1) M^J_{\lambda_a \lambda_b \lambda_c \lambda_d}(s) d^J_{(\lambda_a - \lambda_b), (\lambda_c - \lambda_d)}(\theta) \tag{28}$$

and

$$M^J_{\lambda_a \lambda_b \lambda_c \lambda_d}(s) = \frac{1}{2} \int_0^1 d(\cos\theta) M_{\lambda_a \lambda_b \lambda_c \lambda_d}(s,t,u) d^J_{(\lambda_a - \lambda_b), (\lambda_c - \lambda_d)}(\theta). \tag{29}$$

Comparison of (19, 20) with (28, 29) we see that using helicity states (and only in this case) gives us essentially the same formulae for particles with spin as without. We will use these formulae later in the year when we discuss the weak interactions. Here is a foretaste; consider the electromagnetic reaction $e^+e^- \to q\bar{q}$.

In the limit of zero mass for the external particles (but not necessarily the photon!), the only nonzero matrix elements have $|\lambda_a - \lambda_b| = |\lambda_c - \lambda_d| = 1$. Positive and negative values of $\lambda_a - \lambda_b$, $\lambda_c - \lambda_d$ have equal probability from parity invariance of the electromagnetic interaction.

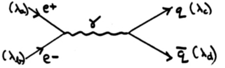

Under those circumstances, the cosθ dependence of the cross section $\propto \sum_{\lambda_a,\lambda_b,\lambda_c,\lambda_d} |M_{\lambda_a\lambda_b\lambda_c\lambda_d}(s,t,u)|^2$ is

$$\begin{aligned} &\propto |d^1_{1,1}(\theta)|^2 + |d^1_{1,-1}(\theta)|^2 + |d^1_{1,-1}(\theta)|^2 + |d^1_{-1,1}(\theta)|^2 \\ &= 1 + \cos^2\theta. \end{aligned} \tag{30}$$

This behavior has been seen at the e^+e^- colliding beams - remember (30) holds at fixed s, i.e., fixed beam energies for e^+ and e^-.

For a typical weak interaction, e.g., $\bar{u}d \to \bar{\nu}_e e^-$

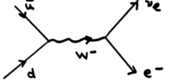

(31)

The W^- does not conserve parity and only couples with $\lambda_a - \lambda_b = \lambda_c - \lambda_d = 1$, i.e., the angular distribution is

$$\begin{aligned} &\propto |d_{11}|^2 \\ &\propto 1 + \cos^2\theta + 2\cos\theta. \end{aligned} \tag{32}$$

The $\cos\theta$ (as opposed to 1 or $\cos^2\theta$) in (31) is characteristic of a parity violating process. (31) is one of the important processes for producing W^-'s in $\bar{p}p$ (pp) collisions. Here quarks and antiquarks are found inside colliding hadrons. In the $\bar{p}p$ case, the $\bar{u}$ dominantly comes from $\bar{p}$ and d from p. The asymmetric decay (32) then shows up as an asymmetry (electron tends to be nearer p than $\bar{p}$ direction) in angular distribution of observed electron. pp scattering will always give a symmetric final state even though subprocess (31) is asymmetric; the ability to test for the asymmetry (and hence the parity violation characteristic of a weak decay) is an important advantage of $\bar{p}p$ colliding beams.